
University of Studies Milano Bicocca
Physics department G.Occhialini

---

Laboratory of Nuclear and Subnuclear measurements

# Muon lifetime and polarization measurement with scintillator detectors in different materials

*By:*

Alessandro Fendillo

Davide Ghittori

---

**ACADEMIC YEAR 2017/2018**

# Contents

# Chapter 1

# Introduction

With this experiment we mean to measure the lifetime of the muons produced by cosmic rays that stop and decay in different materials. Muons and antimuons decay as follows:

$$\mu^- \to e^- + \overline{\nu}_e + \nu_\mu \qquad\qquad \mu^+ \to e^+ + \nu_e + \overline{\nu}_\mu \tag{1.1}$$

Muons are leptons with positive or negative unitary charge, spin $\frac{1}{2}$ and rest mass equal to:

$$m_\mu = 105.658367 \pm 0.000004\,\mathbf{MeV} \tag{1.2}$$

The muons we detect are produced by cosmic rays, which are made out of particles from space and can be classified as:

- **Primary cosmic rays**: they originate from outer space and come form the Sun, other stars or energetic phenomena (novae and supernovae). They are for the most part made of protons ($\sim 95\%$) and Helium nuclei ($\sim 5\%$).
- **Secondary cosmic rays**: produced from the primary cosmic rays interacting with Earth's atmosphere. Mainly made of pions and kaons that then decay into stable particles (electrons, protons, neutrinos etc.) or particles with a lifetime long enough to be observed on Earth (like muons).

So the muons we detect are produced 15 Km above sea level by the secondary cosmic ray mesons decay. To traverse such a distance in a vacuum they need an energy of at least 2.4 GeV, so that their Lorentz factor $\gamma$ is $\sim 23$. Moreover, they lose another 2 GeV to ionization, so their minimum energy needs to be at least 4 GeV to reach Earth's surface. Muons reach sea level with a mean energy of 4 GeV and their angular distribution (for energy higher than 3 GeV) is:

$$\frac{dN}{d\Omega dA dt} \approx I_0 \cos^2\theta \qquad\qquad I_0 \approx 100 \quad \mathbf{m}^{-2}\mathbf{r}^{-1} \tag{1.3}$$

## 1.1 $\mu^+$ decay in materials

The positive and negative muons undergo different interaction with matter depending on the charge, therefore in order to measure the two different lifetimes we have to distinguish muon decays from antimuon ones.

Positive muons decay in materials via weak interaction following the same process showed in 1.1. This decay method can be described by the first order Feynman graph:

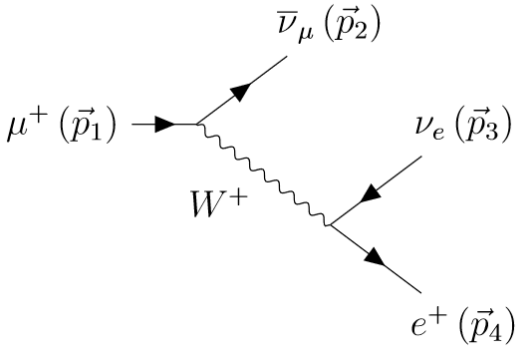


In the low energy limit ($m_W \to \infty$) the matrix element can be obtained from the following relation[1]:

$$M = -\frac{ig_W^2}{m_W^2}[\bar{u}(\vec{p}_3)\gamma^\alpha(1-\gamma_5)v(\vec{p}_4)][\bar{u}(\vec{p}_1)\gamma^\beta(1-\gamma_5)u(\vec{p}_2)]$$

So the differential decay rate in the in the center of mass system ($m_\mu = E_\mu$) is:

$$d\Gamma = (2\pi)^4\delta^4(p_2+p_3+p_4-p_1)\frac{|M|^2}{2E_\mu}\prod_{final\,states}\frac{d^3p_i}{(2\pi)^3}\frac{1}{2E_i}$$

Averaging over the possible spins of initial state and summing over the spins of final states, in the limit of negligible neutrino masses, we obtain :

$$\frac{d\Gamma}{d\Omega} = \frac{2\pi}{3}\frac{G^2}{(2\pi)^5}m_\mu {E_4}^2(3m_\mu - 4E_4)dE_4$$

The total decay rate is the integral of $d\Gamma$ over the whole energy spectrum of the positron ($0 < E_4 < \frac{1}{2}m_\mu$):

$$\Gamma = \frac{G_F^2 m_\mu^5}{192\pi^3} \tag{1.4}$$

The muon lifetime is the reciprocal of the total decay rate and its experimental value is: $\tau_\mu = 2.19714 \pm 0.00007\,\mu s$

## 1.2 $\mu^-$ decay in materials

Negative muons decay differently from their positive counterparts because after slowing down they get caught by the material's atoms and form a muonic atom.
In a model developed by Fermi and Teller, once a muon loses all its kinetic energy it gets caught by the atom and stays for a brief time ($\sim 10^{-13}$ s) in the higher orbital momentum state before rapidly decaying to the quantum state 1s.
The descent causes the emission of Auger electrons and (as the quantum number n gets lower than 5) X rays. Our experimental setup won't be able to detect such radiations due to the threshold chosen for the discriminators.

In their simple model they concluded that the probability $\Lambda_a$ with which the muon gets caught was proportional to the atom's atomic number, according to the "Z law". In a binary compound $A_nB_m$ the relationship between the two $\Lambda_a$s would be

$$\frac{\Lambda_a(A)}{\Lambda_a(B)} = \frac{nA_A}{mA_B} \tag{1.5}$$

Further studies have proven how simplistic this relationship was, neglecting properties of electron shells and atomic structures. Various semi-empiric methods were used to refine the formula.
For the purpose of our experiment it is necessary to accurately predict $\Lambda_a$ because we need to compare lifetimes of $\mu^-$ in materials composed of different atomic species. With salt (NaCl) we use the effective charge instead of the atomic number Z, while the scintillator detectors are composed of $(2CH_3)C_6H_4$ $CH_2$ Polyvinyl-Toluene. The hydrogen is an exception because if it captured a muon it would become a neutral system $\mu$p, which could easily penetrate nearby atoms where the muon would be transfered to due to the higher Z atom. We'll then consider the scintillators composed only of carbon.
Once the muon reaches 1s, it can decay according to (1.1) or be captured by the nucleus. The reaction is:

$$\mu^- + p \to n + \nu_\mu \tag{1.6}$$

and in the Hydrogen is 40,000 times less probable than the other decay. The two start to become equally probable around Z∼11 while in heavier nuclei (Z∼50) the capture becomes prominent (25 times more probable). With carbon the reaction becomes:

$$\mu^- + {}^{12}C \to \nu_\mu + {}^{12}B* \tag{1.7}$$

The subsequent $\gamma$ radiation won't be detected due to inefficiencies in our plastic scintillators.
Finally, the lifetime of $\mu^-$ can be theoretically estimated using[2]:

$$\Gamma_{tot} = \Gamma_{capt} + Q\Gamma_{dec}^{free} \tag{1.8}$$

in which $\Gamma_{tot} = \frac{1}{\tau_{\mu^-}}$, $\Gamma_{dec}^{free} = \frac{1}{\tau_{\mu^+}}$. $\Gamma_{capt}$ stands for the nuclear capture amplitude while Q is the Huff factor, that takes into account the lower decay rate of $\mu^-$ due to its bond with the atom.
$\Gamma_{capt}$ can be theoretically estimated using Primakoff's semi-empiric formula:

$$\Gamma_{capt}(A,Z) = Z_{eff}^4 X_1[1 - X_2(\frac{A-Z}{2A})] \tag{1.9}$$

in which $X_1$ stands for the capture rate of muons in Hydrogen and $X_2$ is a parameter that takes into account Pauli's exclusion principle for nuclei.
Q is always less or equal to 1. Qualitatively we expect the orbiting muon to have a smaller phase space in regards to the free one; consequently its decay amplitude will be smaller in regards to $\mu^+$, as we can see from:

$$\Gamma_{dec}^{free} \propto m_\mu^5 \tag{1.10}$$

$$\Gamma_{dec}^{bound} \propto (m_\mu - \Delta E_B)^5 \tag{1.11}$$

In which $\Delta E_B = \frac{1}{2} m_\mu (Z\alpha)^2$.
For small Z we have that:

$$\Gamma_{dec}^{bound} = \frac{\Gamma_{dec}^{free}}{1 - \beta(Z\alpha)^2} \tag{1.12}$$

Where $\beta \approx 2.5$.
In The following table are shown the values for $\tau_{tot}$ and Q for $\mu^-$ in different materials.

| Element | $\tau_{\mu^-}$ [ns] | Q | Z ($Z_{eff}$) |
|---|---|---|---|
| C | 2026.3 ± 1.5 | 1.00 | 6 (5.72) |
| Na | 1204 ± 2 | 0.996 | 11 (9.95) |
| Al | 864 ± 2 | 0.993 | 13 (11.48) |
| Cl | 560 ± 2 | 0.989 | 17 (14.24) |

Table 1.1: Values of $\tau_{\mu^-}$ in different material

As we expected, muon lifetime in materials is shorter than the free lifetime.

## 1.3 Interaction between muons and matter

When going through matter muons lose energy mainly through collisions with atomic electrons, causing their excitation or ionization. They also lose some energy through radiation. We can approximate the energy lost in a distance $dx$ with:

$$-\frac{dE}{dx} = a(E) + eB(E) \tag{1.13}$$

which is valid for a broad range of E. Ionization is the most common result when dealing with energies ranging from a few MeVs to tens of GeVs (the muon critical energy for C, NaCl and Al is of a few TeVs, while the average energy of cosmic muons is 3 orders of magnitude lower). We can then describe the muon energy loss in materials using the Bethe-Bloch formula (Figure 1.1):

$$-\frac{dE}{dx} = 4\pi N_a r_e^2 m_e c^2 \rho \frac{Z}{A} \frac{1}{\beta^2} [\log \frac{2m_e \gamma^2 v^2}{I} - \beta^2] \tag{1.14}$$

in which $m_e$, $r_e$, $N_a$, $I$, $Z$, $A$, $\rho$, and $v$ stand for, respectively, mass and classic radius of the electron, the Avogadro number, the average ionization potential, the charge, atomic weight and density of the material and the speed of the muon.

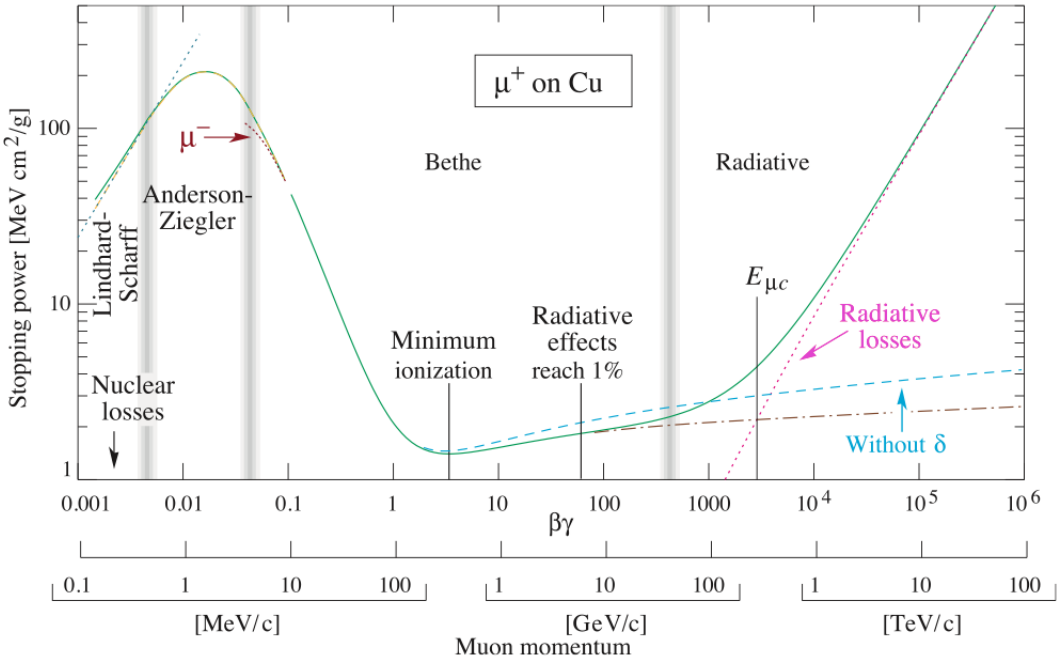


Figure 1.1: Stopping power for anti-muon on a Cu target

# Chapter 2

# Experimental setup

## 2.1 Electronics

In this experiment we used the following electronics:

1. CAEN N1470 - Programamble HV Power Supply;
2. CAEN N1145 - Quad Scaler and Preset Counter;
3. CAEN N93b - Dual Timer (x2);
4. CAEN N108 - Dual Delay (x2);
5. CAEN LRS 622C - Quad Coincidence Unit;
6. CAEN N405 - 3Fold Logic Unit;
7. CAEN N454 4-8 Logic Fan-in-Fan-out;
8. LECROY 429A Logic Fan-in-Fan-out;
9. CAEN N417 8-Channel Low THR Discriminator;
10. $\Sigma^{\text{Silena}}_{\text{Milano}}$ H.V Power Supply Mod. 7720;
11. CAEN NIM-Crate Mod.8304 (12 slot 7U (5+2) switching NIM Crate);
12. TEKTONIX TDS 2022 Two Channel Digital Storage Oscilloscope;
13. GW INTESK Dc Power Supply SPS-1230 (12 V/30 A);

The specifics can be found at the manufacturers' websites.

## 2.2 Scintillator detectors

We use three plastic scintillator detectors ($(2CH_3)C_6H_4$ $CH_2$ Polyvinyl-Toluene) to reveal the passage of muons and ionizing particles produced by the decay.
Muons from cosmic rays have an average energy of 4 GeV, that translates to a Lorentz factor of $\sim 40$, so the particles can by considered MIPs (minimum ionizing particles). The organic scintillators density is close to $1\,\mathrm{g\,cm^{-3}}$, so the energy loss per unit length is $\sim$2 MeV cm$^{-}$1, and they are (80x30x4) cm: in each one will be deposited a minimum energy of 8 MeVs, well above the energy of natural radiation (3 MeV).

## 2.3 Scintillator detectors characterization

The detectors, labeled as PIPPO, TEO and ALICE, must be characterized to determine their optimal work conditions. We initially vary the photomultipliers biases and discrimination thresholds for anodic signals; we then optimize the detection efficiency.

### 2.3.1 Initial setup: single particle rates

The anodic signals sent from the photomultiplier are received by the discriminator, which emits a logic signal every time the anodic signal is above a certain threshold. For this characterization we send the output of the discriminator to the input of a counter.
We choose a bias, then we change the discriminator threshold to find a spot where all the noise from ambient radiation is cut off and we detect just muons and more energetic phenomena. The bias must be high enough to detect all the information of interest but low enough to generate signals accepted by the discriminators (less than 250 mV). With help from the counter we measure how many signals are above the set threshold in an arbitrary amount of time (we chose 30 s, which seemed appropriate given the rate). We expect to obtain a high count for low thresholds (due to natural radiation), then for the count to rapidly decrease and reach a plateau. For higher thresholds, then, the count should approach 0 as less and less muons have enough energy to be detected.
We want to find a reasonably long plateau to set our threshold at, so that even if the setup is subject to small fluctuations, the work conditions stay the same.

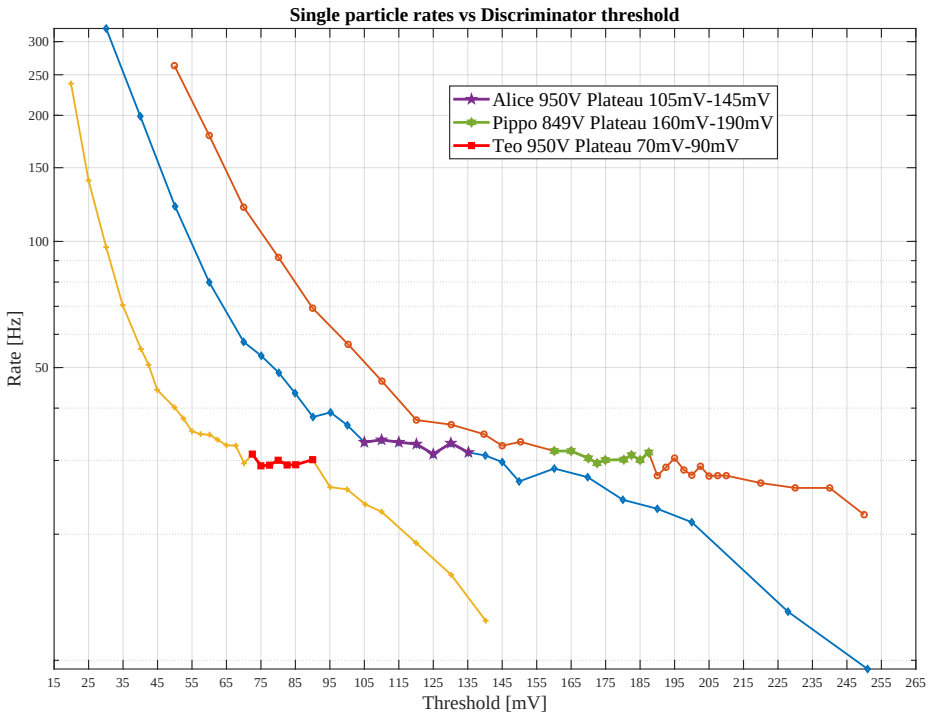


Figure 2.1: Single particle rates (logarithmic) vs discriminator threshold for the three detectors. The plateaus can be seen between 30 Hz and 35 Hz. The particular biases were chosen taking into account the efficiencies measured in section 2.4.

After measuring the efficiency of the detectors at each bias (see section 2.4) we chose:

| Detector | Bias (V) |
|---|---|
| Pippo | 849 |
| Teo | 950 |
| Alice | 950 |

A higher bias translates to a longer plateau and the signals can still be received from the discriminators.

## 2.4 Efficiency

In this section we measure each detector efficiency, showing how it's unrelated to the efficiency of the external detectors used to measure it. We place the examined detector between the other two, aligning them vertically. As before, we send the outputs from each detector to a discriminator (the threshold is set at a plateau). Using a coincidence unit and a counter (Figure 2.2) we measure the rate of triples and the rate of doubles (of the external detectors).

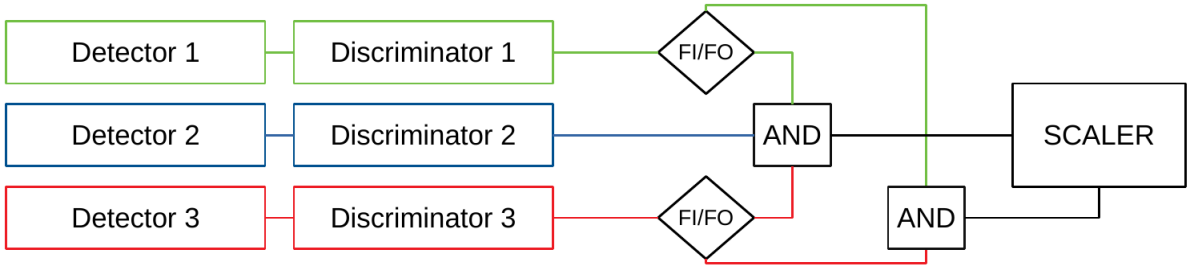


Figure 2.2: Setup used for the efficiency study

The efficiency is given by the ratio of the two, in fact, let's say we define them respectively as $N_{triples}$ and $N_{doubles}$, then

$$N_{doubles} = N\epsilon_1\epsilon_3 \tag{2.1}$$

$$N_{triples} = N\epsilon_1\epsilon_2\epsilon_3 \tag{2.2}$$

$$\frac{N_{triples}}{N_{doubles}} = \frac{N\epsilon_1\epsilon_2\epsilon_3}{N\epsilon_1\epsilon_3} = \epsilon_2 \tag{2.3}$$

in which $\epsilon_n$ stands for the efficiency of the n-th detector.
From our previous study, we select the biases to investigate for each detector:

| Detector | Biases (V) |
|---|---|
| Pippo | 801, 849 |
| Teo | 900, 950 |
| Alice | 900, 950 |

We only test the efficiency at biases that produced a clearly distinct plateau in our preliminary study (Figure 2.1).
First we verify that the efficiency of the detector in the middle is independent from the external detectors threshold. We choose the lowest and the highest thresholds (still in the

plateau) for the external detectors (82.5-100 mV for Alice, 75-90 mV for Teo), then we vary Pippo's threshold between 105 and 127 mV. As shown in Figure 2.3, the measured efficiency stays the same within statistical fluctuations. Each measurement is done over a time of 300 s.

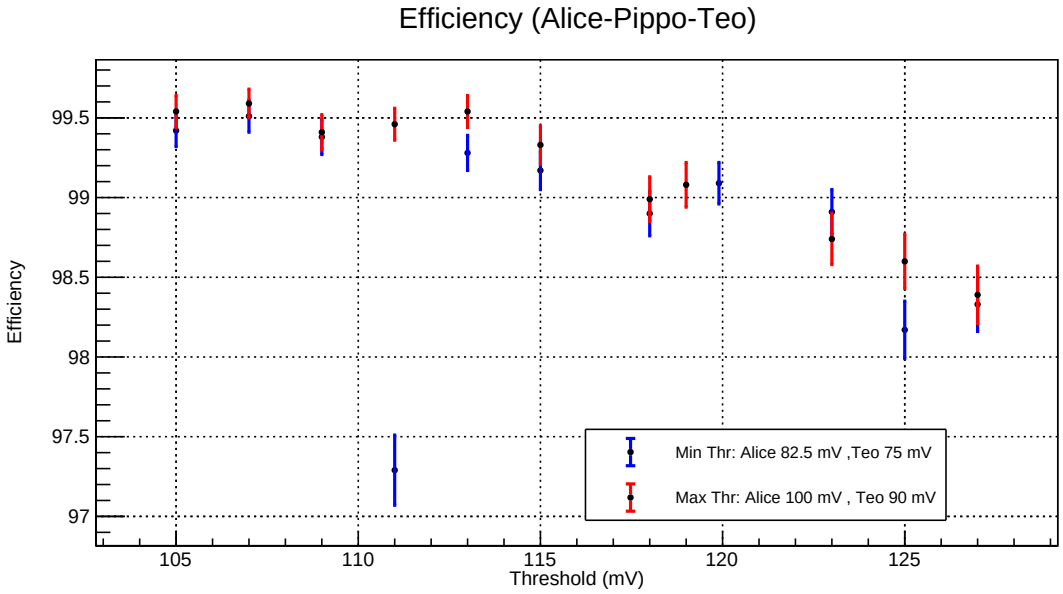


Figure 2.3: Efficiency measurements setting the threshold for the external detectors at the extremes of the plateau. The results are roughly the same for both configurations.

We can then choose a threshold in the middle of the plateau for the external detectors. We proceed with measuring the efficiency of the remaining biases and detectors.

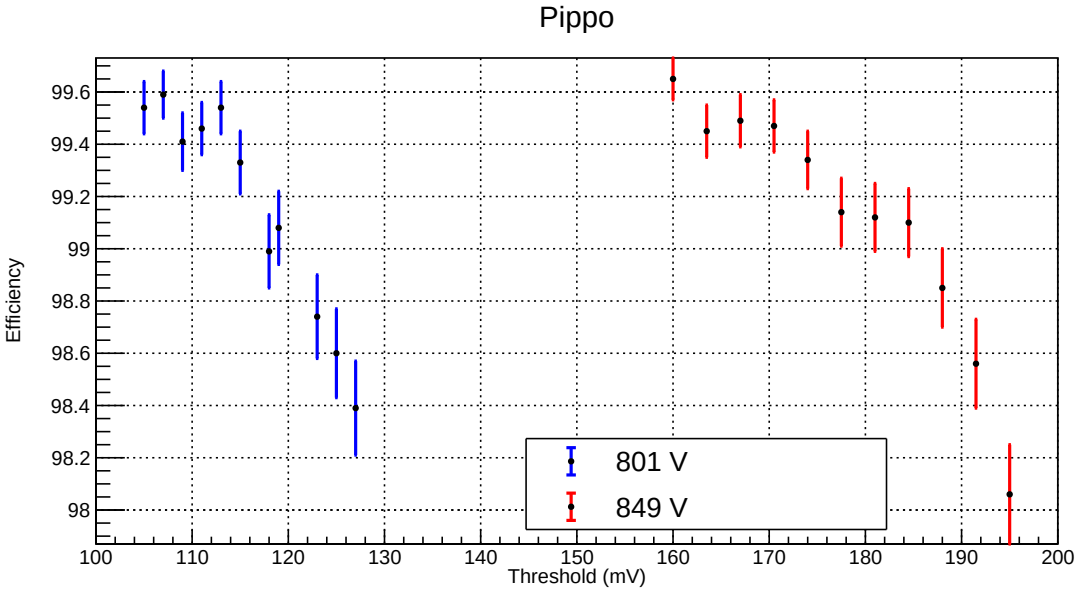


Figure 2.4: Efficiency measurements for detector Pippo.

We obtain similar results both at 801 V (threshold between 114 mV and 128 mV) and at 849 V (threshold between 160 mV and 195 mV): the efficiency of Pippo is around 99.5% at

the start of the plateaus, then drops more or less rapidly as the threshold gets higher. For the following measurements we set Pippo's bias at 849 V and its threshold at 170 mV. For Alice we measure its efficiency at 900 V and 950 V, varying its threshold between 80 mV and 100 mV for the lower bias and between 125 mV and 145 mV for the higher one.

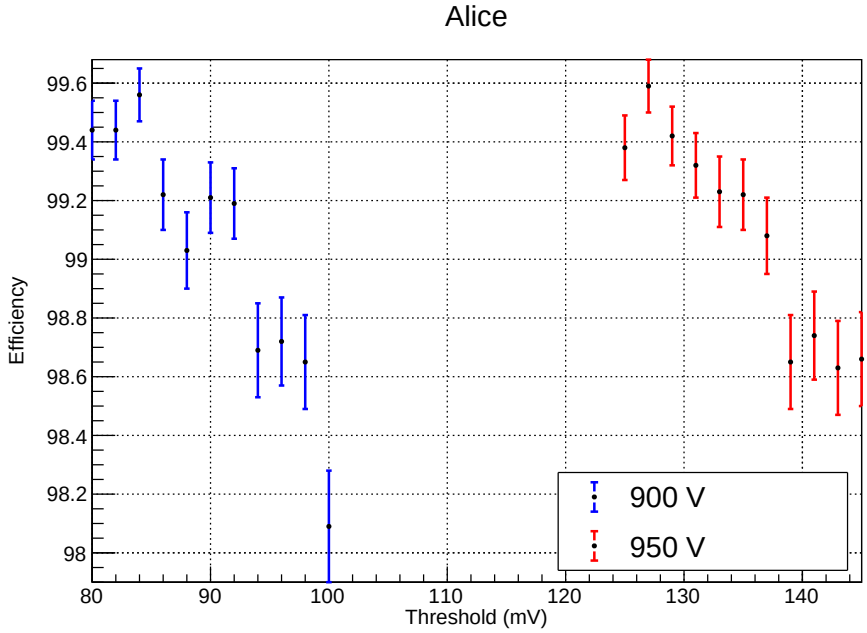


Figure 2.5: Efficiency measurements for detector Alice.

We choose for Alice a bias of 950 V and a threshold of 130 mV.
For Teo, the last one, we measure its efficiency at 900 V and 950 V, varying its threshold between 45 mV and 55 mV for the lower bias and between 70 mV and 90 mV for the higher one.

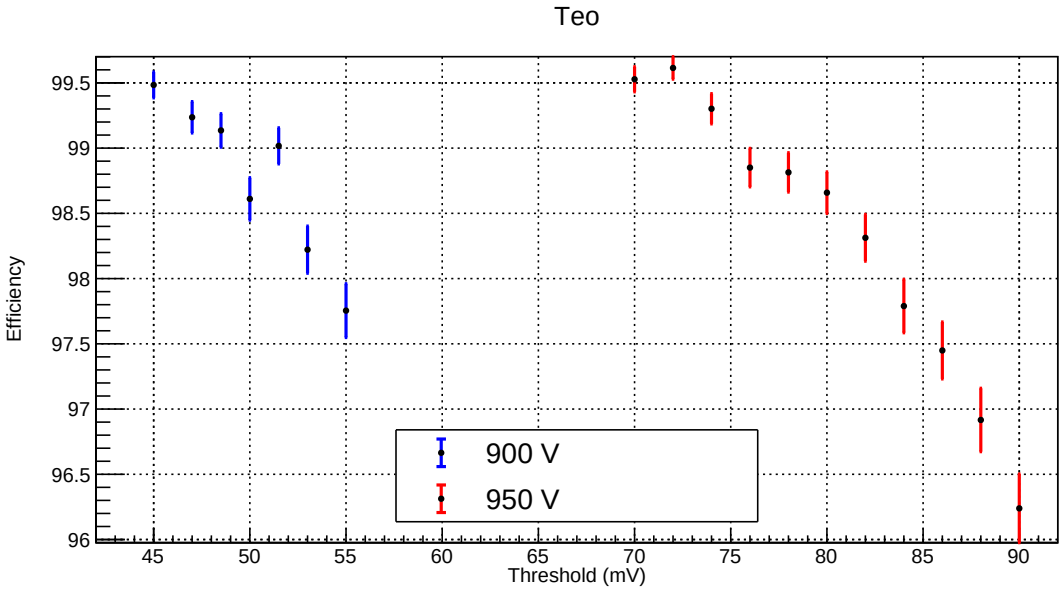


Figure 2.6: Efficiency measurements for detector Teo.

We choose for Teo a bias of 950 V and a threshold of 75 mV.

To collect more data we repeated the measurements with the final setup for each detector, summarized in the following table.

| Detector | Bias (V) | Threshold (mV) |
|---|---|---|
| Pippo | 849 | 170 |
| Teo | 950 | 75 |
| Alice | 950 | 130 |

Before that, we reduced the distance between each detector to 2 cm to increase the geometric acceptance of the setup. We assumed the data to follow binomial distribution: measuring the efficiency $\epsilon$ is like having $N_{doubles}$ tries and counting $N_{triples}$ as successes; $\epsilon$ is then the chance of success. So it follows that the error on the number of triple coincidences is:

$$\sigma_{N_{triples}} = \sqrt{N_{doubles}\epsilon(1-\epsilon)} \tag{2.4}$$

The error on the efficiency can then be obtained:

$$\sigma_\epsilon = \frac{\sigma_{N_{triples}}}{N_{doubles}} = \sqrt{\frac{\epsilon(1-\epsilon)}{N_{doubles}}} \tag{2.5}$$

| Detector | Runtime (h) | Efficiency |
|---|---|---|
| Pippo | 90 | 99.254 ± 0.004 % |
| Teo | 65 | 99.257 ± 0.004 % |
| Alice | 45 | 99.206 ± 0.005 % |

The detectors are similar and the efficiencies are lower than expected from previous measurements

### 2.4.1 Uniformity

After measuring the efficiency of the detectors at different voltage biases we change the setup in order to study the efficiency of different sections of the scintillators.
We place the first detector orthogonally to the others in order to cover only a fraction of the scintillator area. In this way we can analyze three different regions: the farthest one from the photomultiplier (PMT region), the central one and the PMT one.
The scintillators efficiency can vary in these regions due to degradation of the detectors, so we expect to measure different values depending on the covered area.
The second and the third detectors are aligned in the same way as before, so we move the first one through the three regions studying the response of the second scintillator (Figure 2.7).

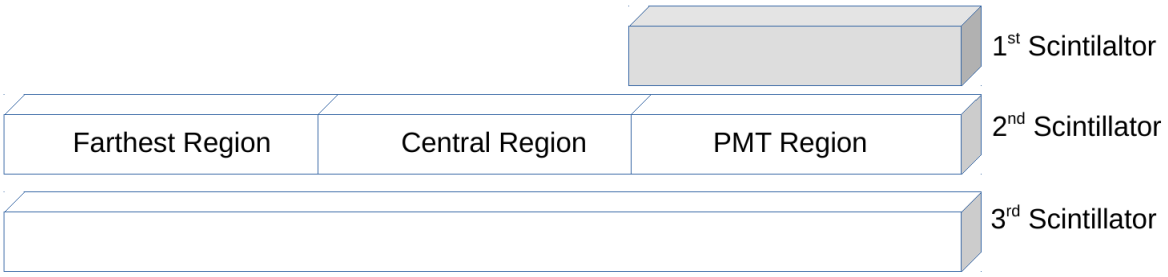


Figure 2.7: Schematic representation of the experimental setup used for uniformity measurements

Using this configuration we measure only the rate of triples and doubles of the area covered by all three scintillators.
Figures 2.8a, 2.8b, 2.8c show the efficiency of the three regions:

- Farthest region: the first scintillator is placed 50 cm from the PMT;
- Central region: the first scintillator is placed 20 cm from the PMT;
- PMT region: the first scintillator is placed 0 cm from the PMT;

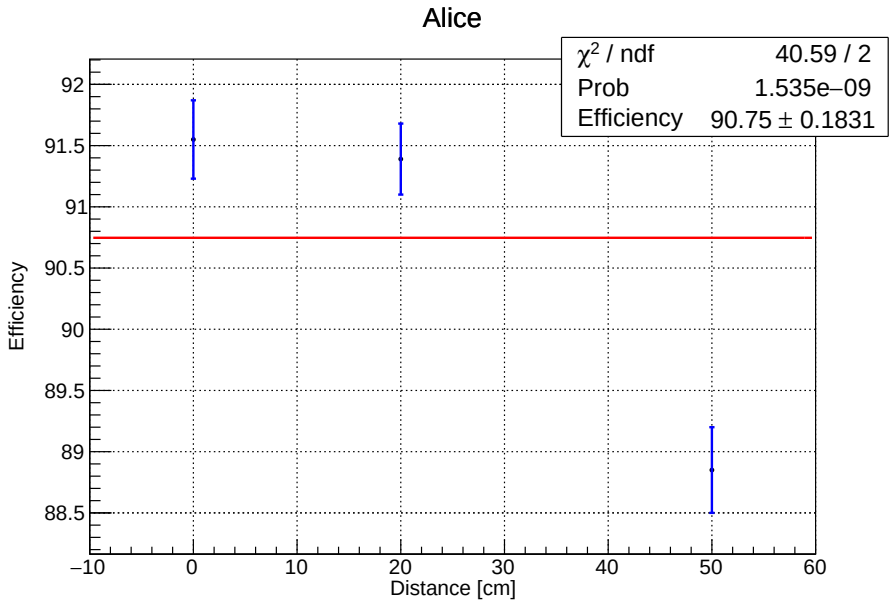


(a) ALICE uniformity measurements

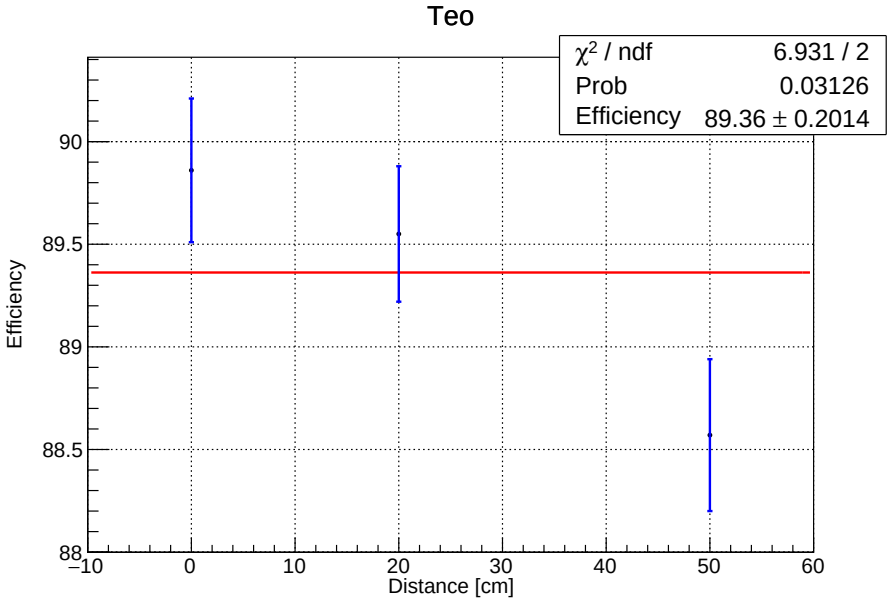


(b) TEO uniformity measurements

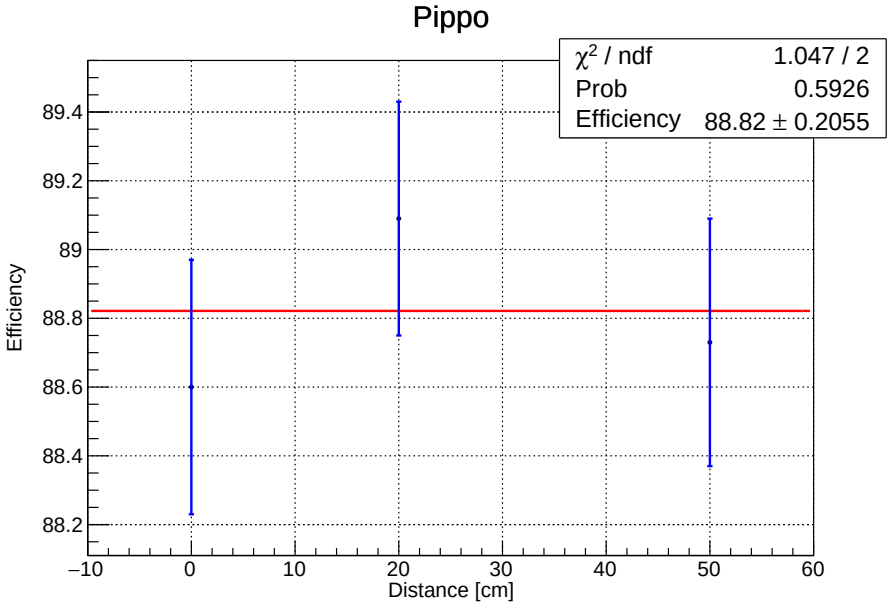


(c) PIPPO uniformity measurements

As expected the three detectors have a non uniform efficiency but the variation in the different regions is less than 2 times the statistical error, except for the farthest regions. In order to compensate the low efficiency of this region we decide to place the detectors so that the farthest region of each one is aligned to the PMT region of the next one.
From these data and the values of efficiency measured in table 2.4 we can conclude that PIPPO has the best performance so we decide to use the following configuration:

1. TEO 1$^{st}$ detector;
2. PIPPO 2$^{nd}$ detector;
3. ALICE 3$^{rd}$ detector;

## 2.5 Electronics characterization

Our goal is to elaborate a specific setup that can perform an analysis of the scintillators signals and give us a logic signal when the inputs satisfy given conditions. The output is used as a trigger in order to decide which signals we have to acquire to measure the muon lifetime.
In this section we'll characterize each electronic instrument employed.
The instruments used are: discriminator, fan-in-fan-out, delay unit, logic unit and a coincidence unit.
The configuration of these instruments is shown in Figure 2.8

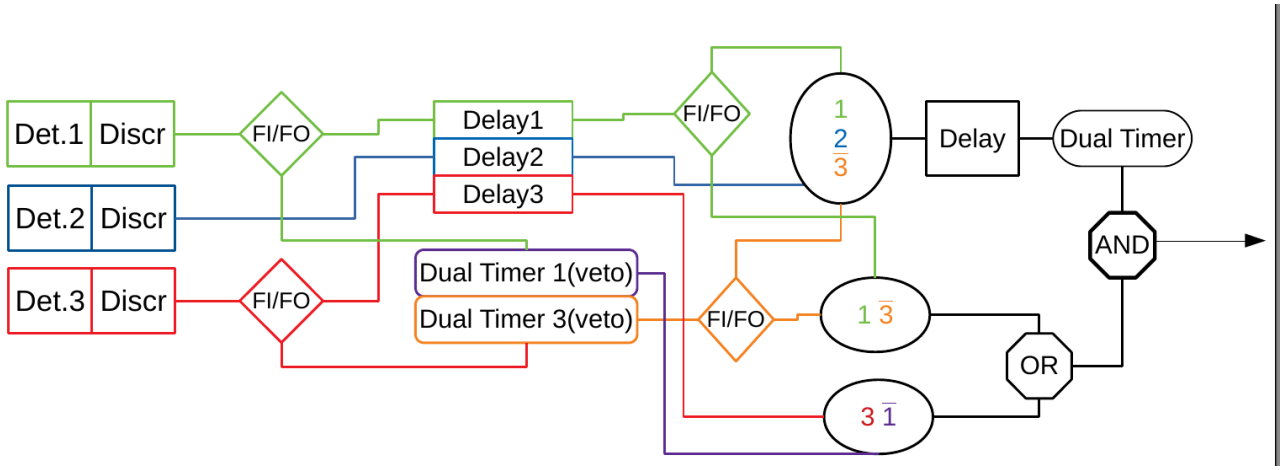


Figure 2.8: Final electronic setup. $\bar{n}$ represent a veto signal obtained from the n$^{th}$ detector

### 2.5.1 Discriminator

The discriminator is used to obtain a logic signal from an anodic one when the input exceed a given voltage value (the threshold). We can act on its threshold, that we have already set (section 2.3.1 and section 2.4), and on the square waves width. This parameter has to be chosen to match the coincidence and logic unit requirements so its optimal values will be determined in following studies.
Possible noise sources of this device are the Amplitude Walk and Time Jitter effects that can modify when the anodic signals exceed the threshold and so when the square waves are produced.
We will see in the next sections that the time width selected is large enough to ignore these effects.

### 2.5.2 Delay unit

The delay unit is a passive instrument used to introduce a time delay between the input signal and the output one.
In order to verify the linearity of this unit we used a fan-in fan-out module to split a logic signal, then using an oscilloscope we measured the time difference between the original signal and the one coming from the delay unit.
Repeating this measurement at different delay values we obtained a linear graph (Figure 2.9). The value of the linear fit at 0 delay corresponds to the intrinsic delay of the device.

We have two different delay units each one with two modules: 108m223 Up and Down, 108m224 Up and Down.

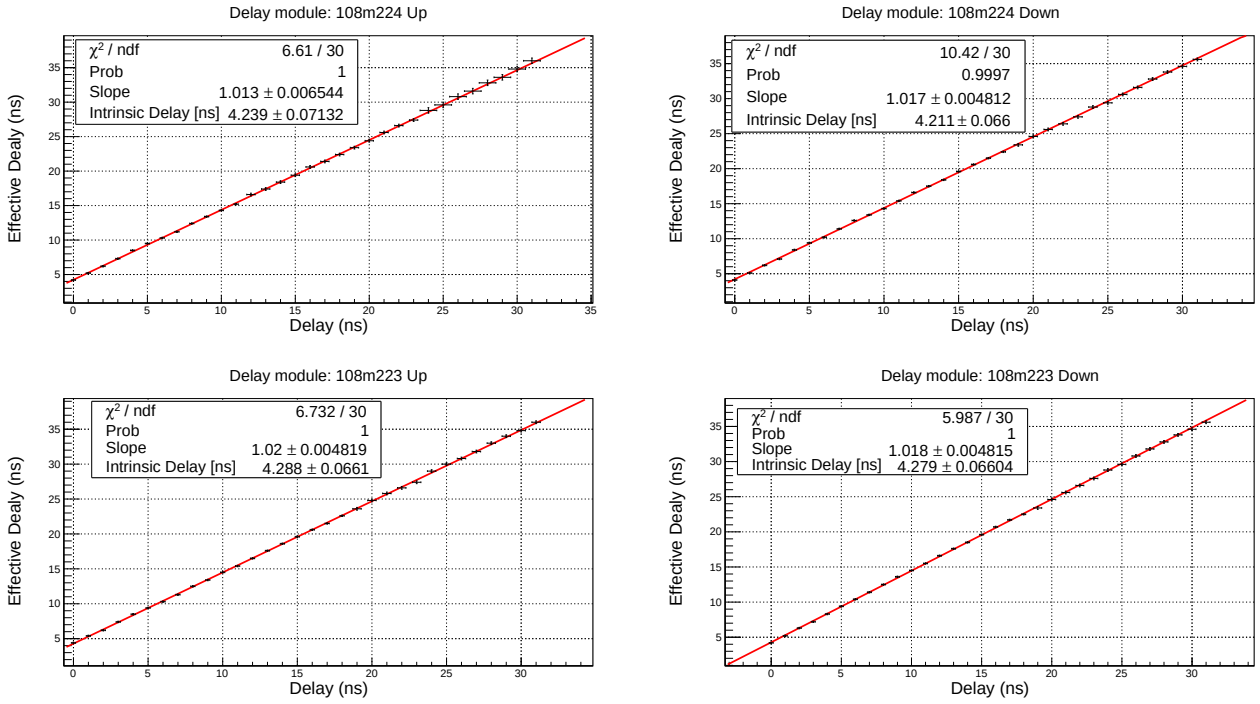


Figure 2.9: Characterization of delay units linearity

### 2.5.3 Logic unit

The logic unit allows us to perform boolean operations (AND, OR or NOT) between logic signals. We want to test the response of the unit when changing the overlap of the input signals (which are NIM standard and 100 ns long).
AND is a function that gives back a logic signal only when the two input signals overlap. We use a single detector whose signals are triplicated with a fan-in fan-out: one of them goes directly into a counter, that gives us the effective number of particles detected, while the other two are the logic unit input signals. The output from the logic unit goes into another counter. We delay one of the input signals and change the delay until we receive no signal from the coincidence unit. We measure the ratio between the unit positive responses and the total particles detected. We expect that for a delay lower than 100 ns the ratio is 1 and for a higher delay the ratio is 0. However the unit needs a minimum overlap between input signals to properly function; this leads to the unit's response not being a perfect step.

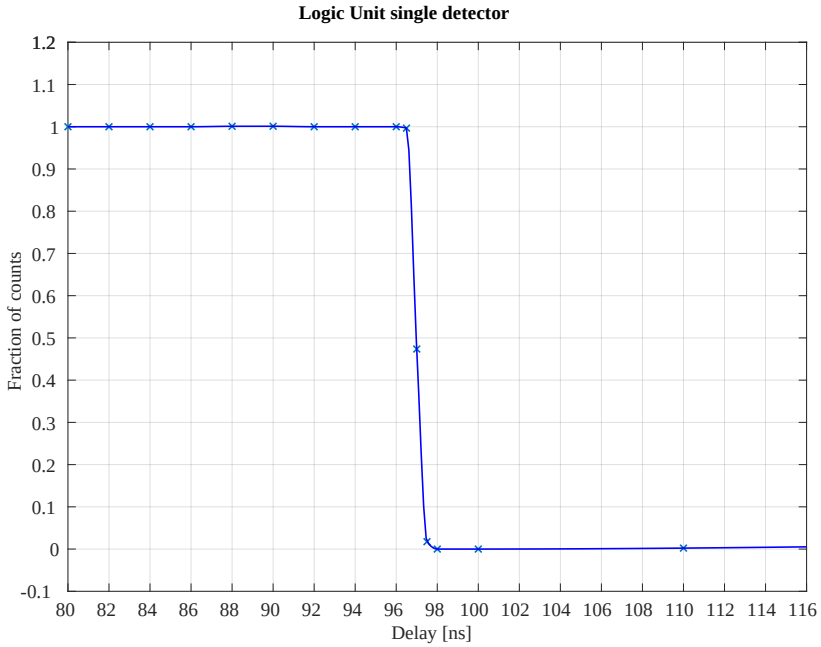


Figure 2.10: Ratio of positive results of the AND operation vs input signals delay. A single detector was used.

We infer that the logic unit needs a 4 ns overlap between the input signals to consider them synchronous. The need to receive signals between multiple detectors adds to the minimum overlap necessary: to evaluate how much, we repeat the measurement using both Alice's (delayed) and Teo's signals as input for the AND operation. This time we count how many prompt coincidences we obtain in 1 minute, changing the delay as before.

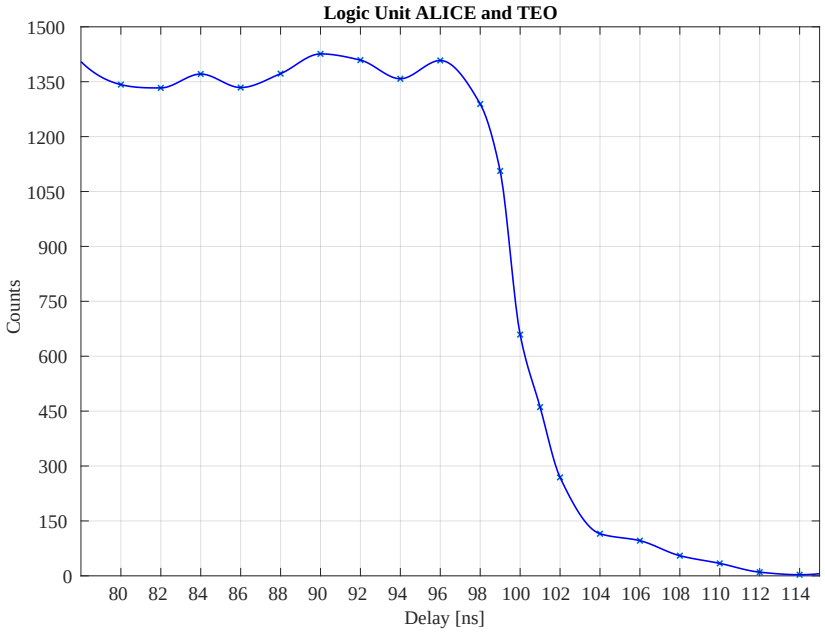


Figure 2.11: Ratio of positive results of the AND operation vs input signals delay. Two detectors were used.

We notice that this time the slope does not go to zero as quickly as before. Even when the second signal is delayed more than 104 ns we have some amount of prompt coincidences. This seems to indicate that the relative intrinsic delay between the signals coming from the two detectors can fluctuate by an amount of at least 10 ns.
We point out that, given a count rate of 30 Hz, the probability of having a random coincidence in $t = 100$ ns is next to zero.

Next we characterize the behavior of the unit veto function, which is needed to perform the NOT operation. One of the inputs of the unit acts as a veto: whenever the unit receives an input signal from another port it will send an output signal unless a veto signal is also present. To test this function we used Alice's signals as the veto input and Teo's as the other input. We wanted the veto signal to be at least 50 ns larger than the other one, so we modified the output from Alice's discriminator to be 132 ns long and Teo's to be 80 ns long. We also duplicated Teo's signals and sent them to a counter to know the ratio between transmitted and total signals.
First we delayed Teo's signals until they were no longer blocked, then we reversed the setup and delayed the veto (that's the reason for negative delays in picture 2.12).

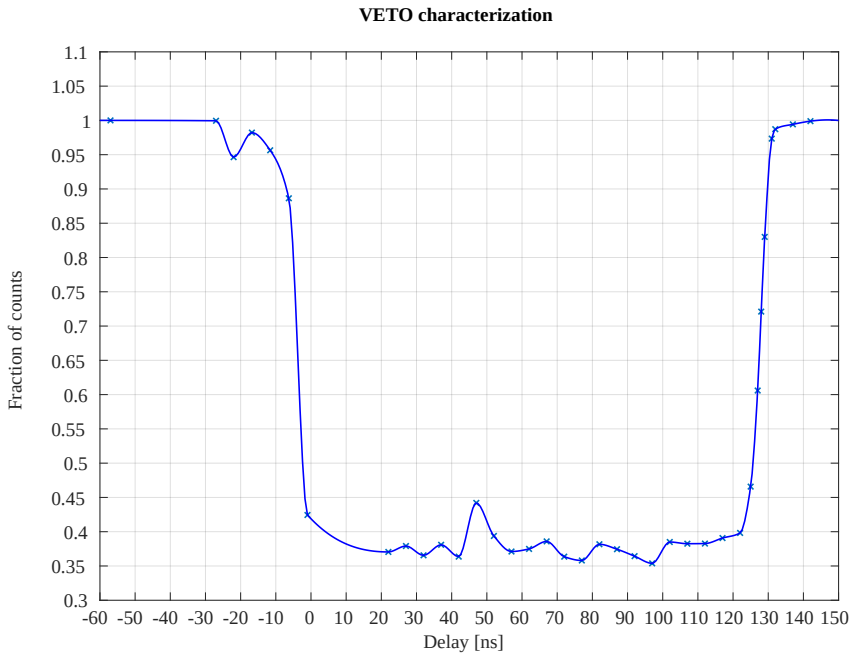


Figure 2.12: Characterization of the logic unit veto function.

We expected the veto to work when the input signal was completely inside the veto signal, but that is not the case: the only requirement for the signal to be blocked is that it arrives when the veto is already present. There is no need for the veto signal to be significantly larger than the one it wants to negate but, taking into account random fluctuations in the time delay between two signals, we need a small delay (∼15 ns) on the input signal.

### 2.5.4 Coincidence unit

We repeat the measurements done for the AND function of the logic unit, this time for the coincidence unit, obtaining similar results.

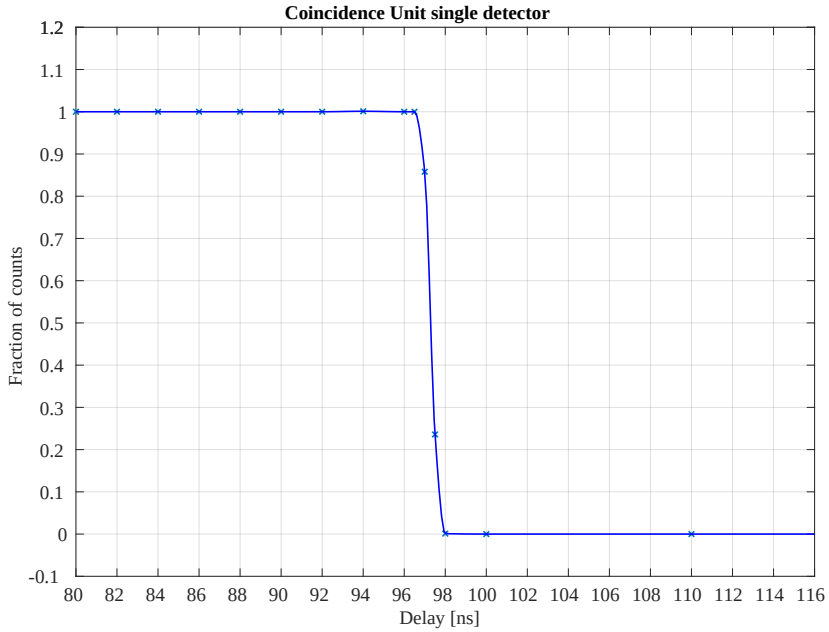


Figure 2.13: Ratio of positive results of the AND operation vs input signals delay. A single detector was used.

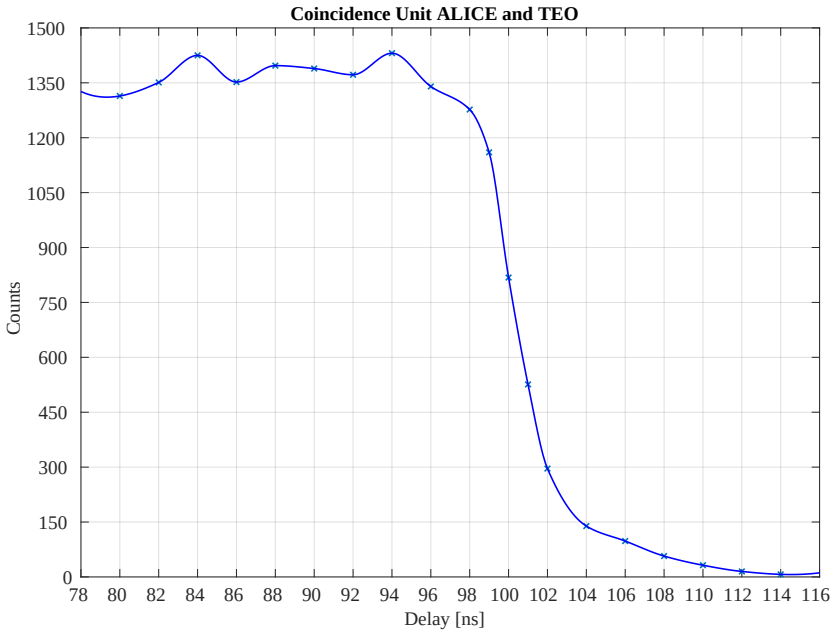


Figure 2.14: Ratio of positive results of the AND operation vs input signals delay. Two detector were used (ALICE and TEO).

Once again, using two detectors increases the delay needed not to have false positives for the AND operation, while the single detector measurement still shows that the coincidence unit needs the two signals to overlap by at least 4 ns.
We won't use this unit for its veto function.

## 2.6 Trigger signal

In order to perform this analysis we want to observe muons decay in their rest frame so we are interested only in the muons that can lose all of their energy in our detectors.
Our system is designed to discern the muons that lose their energy in the first detector and decay in the second one. The results of the decay are two neutrinos, that cannot be detected, and an electron that is detected by scintillator 1 (TEO) or 3 (ALICE). The events we're looking for are:

1. **START**: the muon arrives and stops in the second detector. This event is characterized by a signal in the first two detectors (TEO & PIPPO) and no signal in the third one (ALICE);

2. **STOP**: the effect of the electron. We search for a signal in the first detector and no one in the third detector or vice versa;

We split our setup into 2 branches: the **START**, that will deal with the start signals, and the **STOP**, that will determine the stop triggers (Figure 2.8).
The start signals are detected using the operation **AND** of the coincidence unit between signals coming from TEO and PIPPO's discriminators.
Then we perform the **NOT** operation between the result of the previous one and the signal coming from ALICE's discriminator. This configuration gives a logic output only when the two conditions are met.
The **STOP** signals require the combination of the operations **OR** and **NOT**: the presence of the electron in the first detector is represented by the **NOT** operation between TEO's signals and ALICE's, similarly the electron passing through the third detector is represented by the same operation switching ALICE and TEO. The **OR** operation between the two previous ones allows us to select the signals that satisfy at least one of the two conditions.
This signals are represented in Figure 2.15.

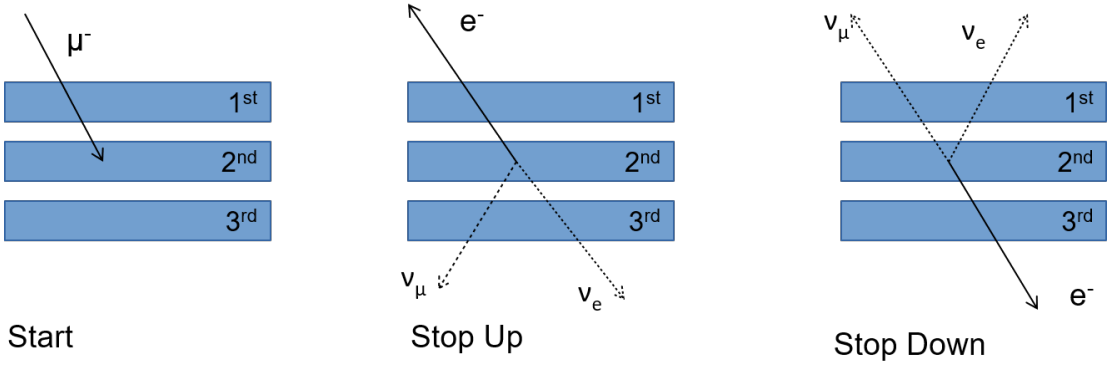


Figure 2.15: Representation of the START and STOP signal. The stop signals are divided in Up and Down depending on the scintillator that detects the electron.

We are interested in START and STOP signals that have a time difference of at most $10\,\mu s$. We chose this value because the muon lifetime is $\sim 2\,\mu s$ so the probability of one living longer than $10\,\mu s$ is negligible. In order to obtain this condition we perform a delayed coincidence between the signal of the START branch and the STOP one. Using

a dual timer we widen the output signals of the START branch to $10\,\mu s$ and use them as input of the coincidence unit. The STOP branch signals are used as second input and an **AND** operation is performed.
However using this system all the signals that satisfy the START branch will satisfy the STOP one too (the START branch requires TEO AND PIPPO NOT ALICE, that also meets one of the two conditions of the STOP branch: TEO NOT ALICE). In order to solve this problem we delay the START branch output by $\sim 100\,ns$ so that only the real decay events are collected, discarding prompt coincidences. However, this means that we won't be able to acquire data on muons that die sooner than that.
In this way we can accomplish our goal: we obtain a trigger signal only when the given conditions are met. This trigger signal tells the oscilloscope when to acquire the data coming from TEO and ALICE's discriminators. Using a computer we can perform a real time analysis and save the acquired data.

### 2.6.1 Detection setup

In this section we'll discuss the choices made on the delay between the signals and their width. We need our detection setup to be sensible on small scales of time and to be stable when dealing with random fluctuations from the detectors.
To avoid start-ups, we can't use narrow signals. What's more, prompt detections from different scintillators can have intrinsic delays by up to $15\,ns$. For those reasons we decide the discriminators outputs to be $100\,ns$ long, while we use a dual timer unit to lengthen the vetoes to $150\,ns$ and the STOP window to $10\,\mu s$: we want to be able to detect most of the muons that stop and decay in the second detector. Each signal going into a NOT operation is delayed $\sim 100\,ns$ from its respective potential veto to account for the aforementioned fluctuations.

# Chapter 3

# Lifetime measurement in materials

## 3.1 In-detector decay

We set up a trigger to detect muons that stop and decay in the $2^{nd}$ scintillator. The online analysis software is able to recognize whether the resulting electron goes through the first or the third detector and how much time passes between the start and the stop signal.
Since $\mu^-$ can be captured by the carbon nuclei (or form bound states), we expect them to have $\tau_{\mu^-} = 2.0263 \pm 0.0015\,\mu s$. On the other hand, positive muons are not subject to the same processes and decay as free particles: $\tau_{\mu^+} = 2.197\,\mu s$.
Once collected the data from the decays, we fill a histogram with the measured muon lives and fit with an exponential function:

$$\frac{dN}{dt} = N_0 e^{-\frac{t}{\tau_{free}}} + C \tag{3.1}$$

in which $\tau_{free}$ is a value we expect to be between $\tau_{\mu^+}$ and $\tau_{\mu^-}$, $N_0$ is heavily dependent on the binning and C parametrizes eventual background events. Most of these are caused by an event in 1 or 3 unrelated to a muon stopping or passing through 1 and 2. This isn't exceedingly improbable given that, in a $T = 10\,\mu s$ time frame the probability of having a stop signal unrelated to a start one is given by[3]:

$$P = (1 - e^{-r_1 T}) + (1 - e^{-r_3 T}) \tag{3.2}$$

in which $r_1$ and $r_3$ are the single particle rate of the respective detector. Since $r_i T \ll 1$

$$P \simeq (r_1 + r_3)T \tag{3.3}$$

so that for every bin $\Delta T$ wide, if $\Delta T \ll T$,

$$P_{bin} \simeq \frac{dP}{dT}\Delta T = (r_1 + r_3)\Delta T = constant \tag{3.4}$$

However, most of the background can be rejected along with the events characterized by two or more potential stop signals, so we expect C to be close to 0. To understand what to expect of $\tau_{free}$ we ran a Montecarlo simulation. We split the same number of events we collected $N$ into $N_{\mu^+}$ antimuon events (probability: 56%) and $N_{\mu^-}$ muon events with a binomial distribution, then we generated $N_{\mu^+}$ events with lifetime $\tau_{\mu^+}$ and $N_{\mu^-}$

with lifetime $\tau_{\mu^-}$. We fill a histogram with all the events and fit it with 3.1. We repeat the procedure a number of times to obtain a statistical expected value to compare with the experiment. We repeat the simulation using different percentage splits of $N_{\mu^+}/N_{\mu^-}$, evaluating the contribution on the uncertainty of $\tau_{free}$ obtaining:

$$\tau_{free} = 2.094 \pm 0.013\,(\text{stat}) \pm 0.003\,(\text{syst})\,\mu s \tag{3.5}$$

### 3.1.1 Experiment results

We collected about 40,000 events in 300 hours. We used the parameters evaluated with the Montecarlo simulations in order to optimize the fitting process.
Due to the finite resolution of our system, the data are not represented by a perfect exponential distribution but they have a cut-off related to the delay used in the electronic setup, already mentioned before. So we have developed an algorithm to choose the best value of binning and the range of the fit in order to improve the analysis.
The contribution of this effect is limited to the first ∼100 ns of the graph so we fixed the higher limit of the fit range and searched for the best value of $\chi^2$ varying the number of bins and the range of the fit.

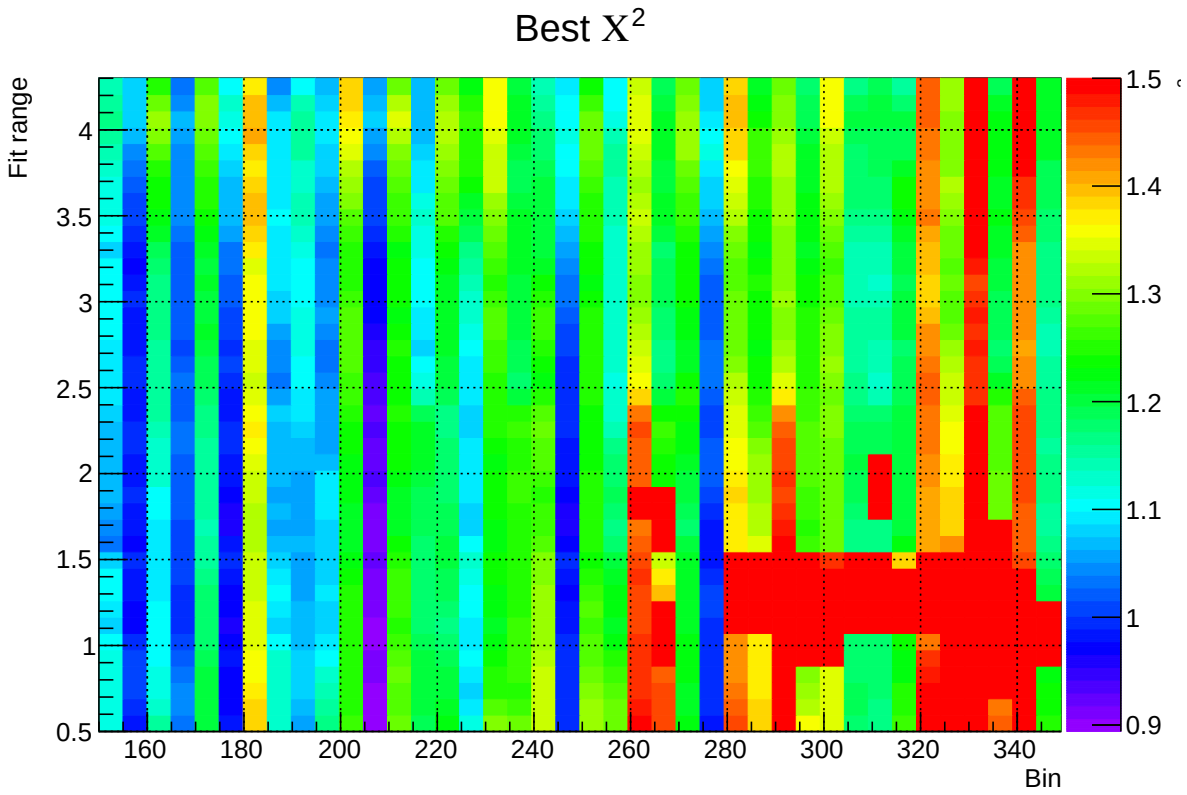


Figure 3.1: Variation of $\chi^2$ depending on the number of bins and the fit range

We chose to vary the number of bins from 150 to 350. For each value of binning we analyzed the $\chi^2$ shortening the range by 0.2 ns: from 0.5 ns to 4.5 ns. The best results were obtained with a number of bins $\text{Bin}_{best}$ equal to 310 and the range of the fit starting at 0.7 ns.
Furthermore, in order to test the stability of the fit, we have studied the value of $\tau_{free}$ depending on the fit range using the optimal number of bins. We repeated this study

using the best fit range and varying the binning. The results of these studies are shown in the following graphs:

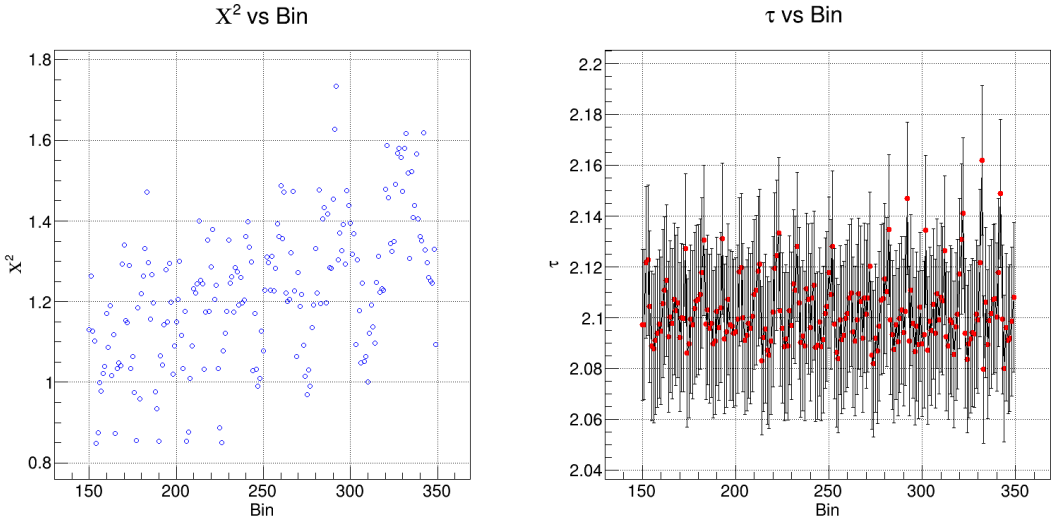


Figure 3.2: Values of $\chi^2$ and $\tau_{free}$ depending on the number of bins. The fit range chose is [0.7 , 9]

Although the $\chi^2$ varies from 08 to 1.6, the value of $\tau_{free}$ is quite stable showing only a slight contribution to the evaluation.

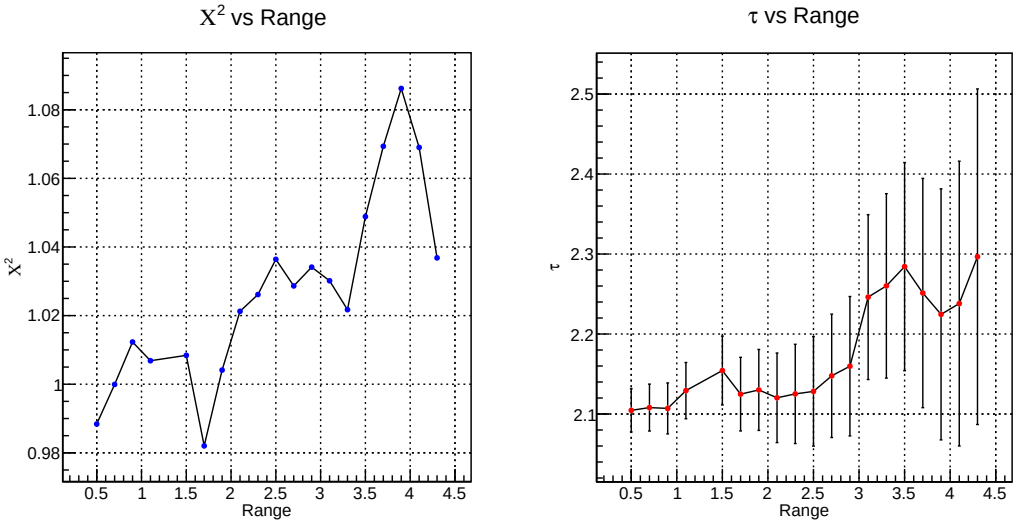


Figure 3.3: Values of $\chi^2$ and $\tau_{free}$ depending on the fit range. The binning is chosen to be 310.

The contribution of the fit range is more accentuated than the previous one, furthermore we can observe that larger fit ranges lead to a better response, not only because we have better values of $\chi^2$ but also because of the higher precision $\tau_{free}$ is evaluated with.

We obtained the following graph:

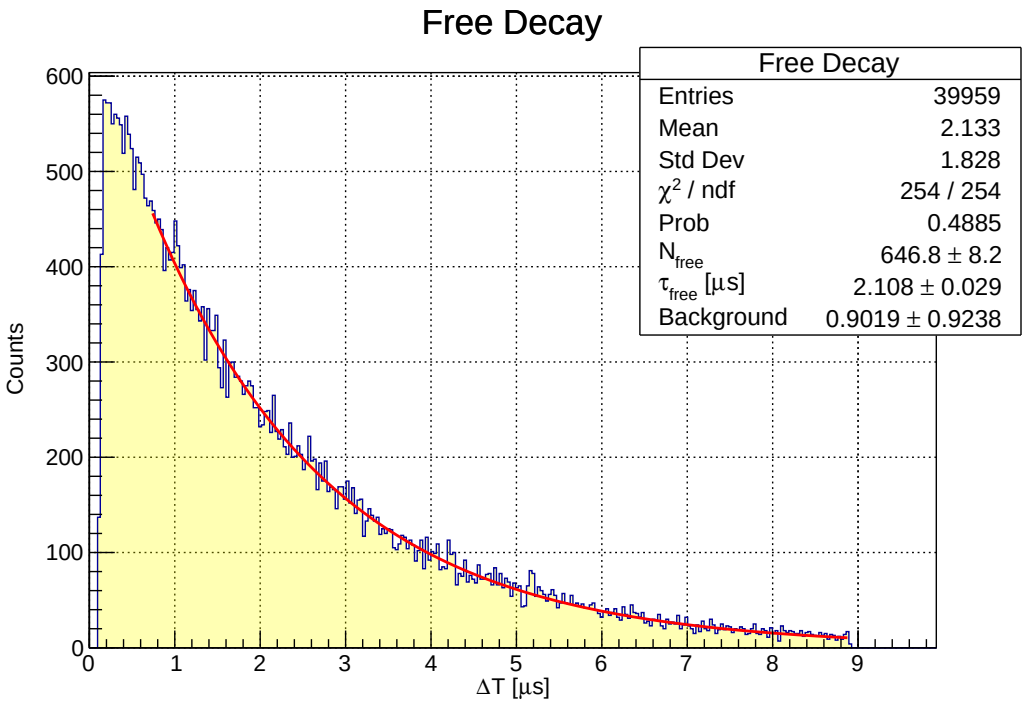


Figure 3.4: Fit of 39,959 events using a number of bin equal to 310. The fit range is [0.7 , 9].

The free muon lifetime evaluated from the data is:

$$\tau_{free} = 2.108 \pm 0.029\,(\text{stat})\,\mu s$$

As we expected, the background is negligible and the parameters show a good agreement with the ones evaluated with the Montecarlo simulation (3.5).

### 3.1.2 $\tau_{\mu^-}$ measurement

In this section we fit the same data with the following function

$$N(t) = N_{\mu^+} e^{-\frac{t}{\tau_{\mu^+}}} + N_{\mu^-} e^{-\frac{t}{\tau_{\mu^-}}} \tag{3.6}$$

trying to separate the two different statistics. Positive muons decay as free muons, while negative muons have a shorter lifetime because they decay by interacting with the detector material. We arrange for $\tau_{\mu^+}$ to be close the measured value of $2.197\,\mu s$ and, while the absolute values for $N_{\mu^\pm}$ depend on the total number of entries and the binning, we force their ratio to be similar to the muon/antimuon ratio (56%-44%)[4]. We leave $\tau_{\mu^+}$ free.

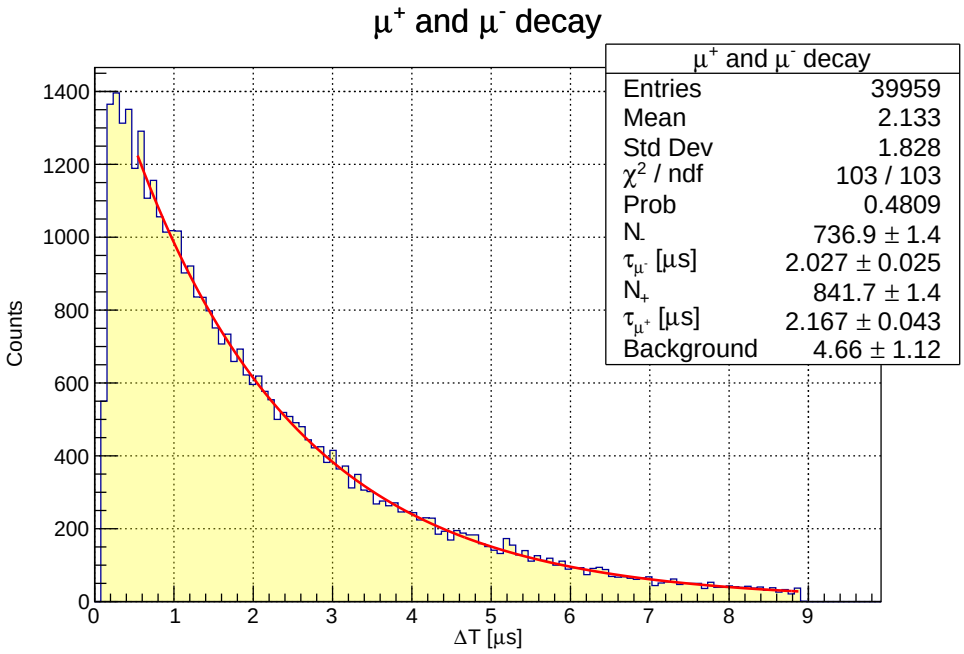


Figure 3.5: Fit for the separate decay of positive and negative muons.

We vary the ratio between muon and antimuon by ±4% (40%-60% and 48%-52%) in order to evaluate the systematic error as difference between the reference value and the new ones.
So we conclude that:

$$\tau_{\mu^-} = 2.027 \pm 0.025\,(\text{stat})\,^{+0.014}_{-0.013}\,(\text{syst})\,\mu s \tag{3.7}$$

which is in agreement with the muon lifetime in carbon (as seen in table 1.1), $2.026\,\mu s$.

## 3.2 Eventual systematic errors

### 3.2.1 Up and down decays

The electron produced from the decay can be seen by the detector 1 (up) or 3 (down). We are able to store this information during the online analysis, so we can look for systematic errors caused by the differences between detectors or by the experiment geometry. Assuming the up and down events follow binomial distribution, we obtain the fraction of up events:

$$f_{up} = 48.1 \pm 0.2\% \tag{3.8}$$

So we can estimate $\tau_{free}$ separately for up and down events, obtaining

$$\tau^{up}_{free} = 2.106 \pm 0.042 \qquad \tau^{down}_{free} = 2.098 \pm 0.040 \tag{3.9}$$

which are in complete agreement with $\tau_{free}$, within statistical uncertainty. We are lead to believe that eventual systematic errors due to the geometry of the experiment or the differences between detectors 1 and 3 are negligible, compared to the statistical error.

### 3.2.2 Dead time losses

Here we quantify the effect of dead time on data acquisition. The trigger system has a dead time of $\sim 10^{-5}\,s$, which is inconsequential compared to the time it takes for the signal to be acquired by the computer.
We acquired 40412 events in 300 hours, so the measured rate of events is:

$$R_m = 3.74 \times 10^{-2} Hz \tag{3.10}$$

Let's suppose the distribution of events is poissonian, then it should follow[3]:

$$I(t)dt = re^{rt}dt \tag{3.11}$$

in which r stands for the event rate. I(t) is the probability of having, given an event at $t = 0$, another event at t. We can estimate the effective trigger rate with the fit in Figure 3.6.

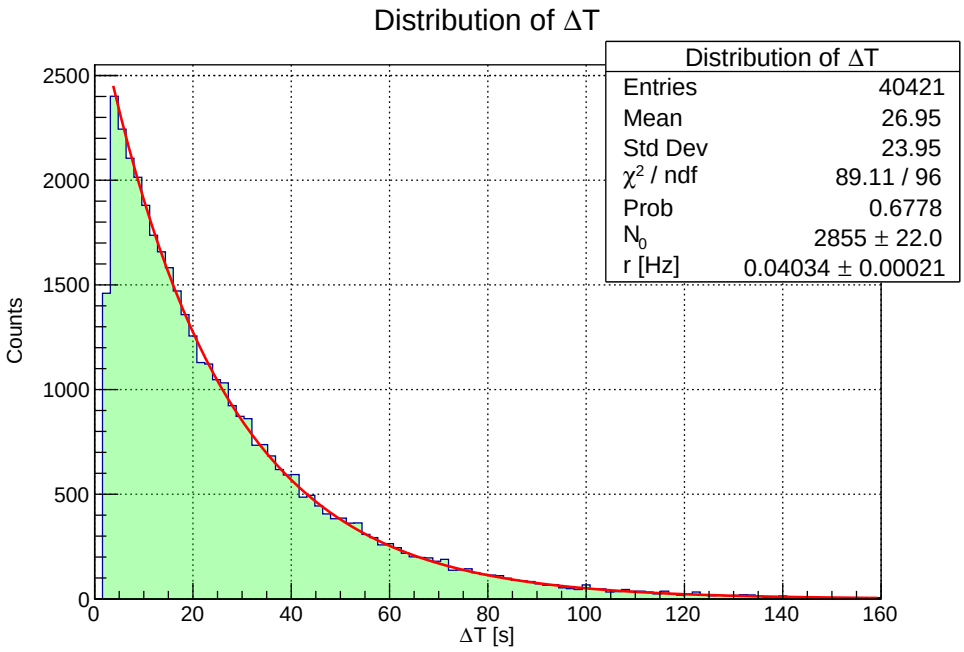


Figure 3.6: Distribution of temporal intervals between one event and the next.

$$R_{eff} = (4.03 \pm 0.02) \times 10^{-2}\, Hz \tag{3.12}$$

The effective rate is, as expected, higher than the measured one due to dead time losses. We want to quantify the pile-up effects and verify that they are consistent with the observations. To determine how much time the acquisition process requires we split the analysis software in its individual functions, measuring each one separately:

- Requesting data from the oscilloscope: $\sim 1.4$ s
- Saving channel 1 data: $\sim 0.04$ s
- Analyzing channel 1 data: $\sim 0.005$ s

- Saving channel 2 data: $\sim 0.04$ s
- Analyzing channel 2 data: $\sim 0.005$ s
- Saving analysis results: $\sim 0.04$ s
- Other: $\sim 0.07$ s

We expect the minimum time between events to be $t_{min} = 1.6\,\mathrm{s}$ and this seems to be confirmed by figure 3.6. Assuming the PC to be a non-paralyzable system, the acquisition rate is[3]

$$R_{exp} = R_{eff} e^{-R_{eff} t_{min}} \tag{3.13}$$

from which we obtain $R_{exp} = (3.78 \pm 0.02) \times 10^{-2}\, Hz$ that is in agreement with $R_m$. We conclude that the acquisition time is responsible for the loss of $\sim 6.2\%$ of the events. We could be more efficient either by analyzing the data offline or by not saving channel 1 and 2 data. Each one of these methods results in a $t_{min}$ of 1.5 s, that only leads to gaining another $\sim 0.2\%$. We believe this loss to be uniform across the decay spectrum, so it only impacts the total statistics acquired.

## 3.3 Muon decay in aluminum

Here we try to study the decay of negative muons in aluminum. We expect $\tau_{Al}$ to be $864 \pm 2\, ns$.
We insert an aluminum slab 3 centimeters thick between detectors 2 and 3. As before, the muons that decay in the $2^{nd}$ scintillator or in the aluminum will trigger an acquisition. The resulting spectrum is a superposition of the $\tau_{free}$ distribution (seen in Figure 3.4) and another exponential distribution with $\tau_{Al}$. We parametrize the fit function as

$$N(t) = N_{free} e^{-\frac{t}{\tau_{free}}} + N_{Al} e^{-\frac{t}{\tau_{Al}}} + C \tag{3.14}$$

where C is the previously discussed potential background, due to accidental coincidences. To improve the fit process we limit the value of $\tau_{free}$ using the one previously evaluated and its statistical error. The analysis results are shown in Figure 3.7. The choices of binning and fit range are made using the same procedure as before.

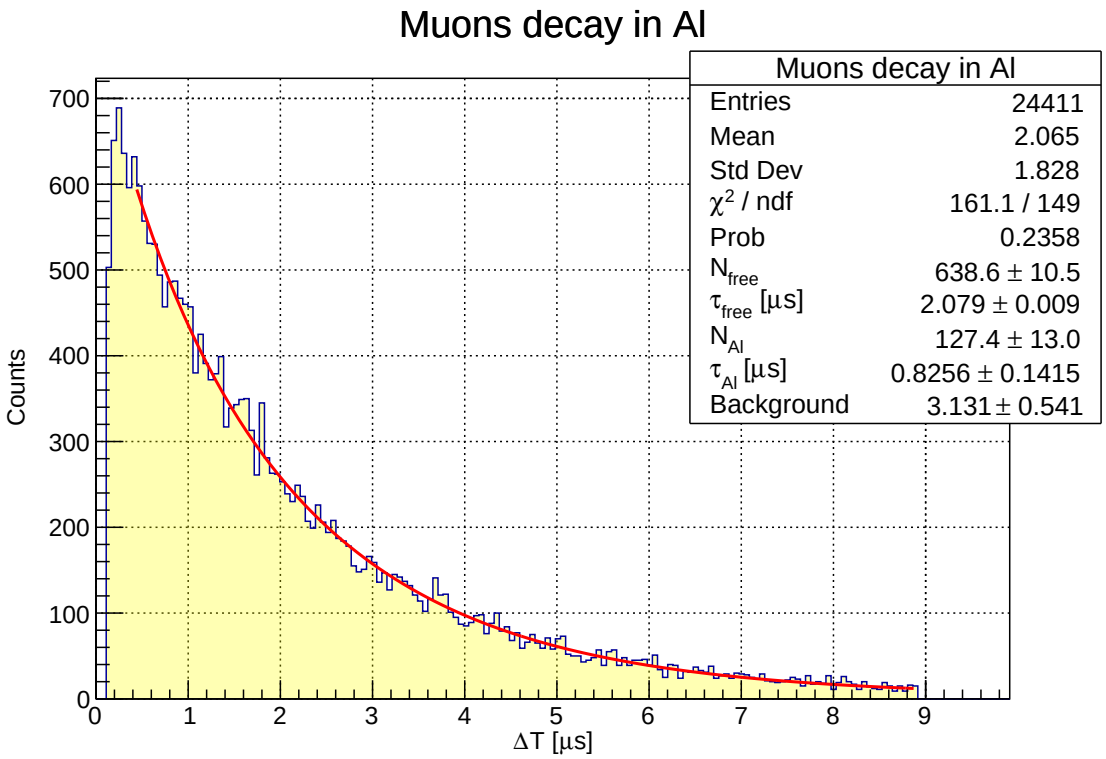


Figure 3.7: Muons decay in aluminum

We collected 24441 events in 144 hours. The result is:

$$\tau_{Al} = 0.826 \pm 0.142\,(stat)\,\mu s \tag{3.15}$$

We also evaluate muon lifetime considering separately up and down decays. The results are:

$$\begin{aligned} \tau_{Al}^{up} &= 0.894 \pm 0.067\,\mu s \\ \tau_{Al}^{down} &= 0.825 \pm 0.056\,\mu s \end{aligned} \tag{3.16}$$

## 3.4 Muon decay in NaCl

To study negative muons decay in NaCl we insert a 5 cm thick layer of table salt between detectors 2 and 3. The expected result for $\tau_{NaCl}$ is evaluated taking into account both chemical species: we'll call $P_{Na}$ the probability that the muon decays in a bound state with the sodium atom and $P_{Cl} = 1 - P_{Na}$ the probability that it instead decays in a bound state with the chlorine. The total decay amplitude is:

$$\Gamma_{NaCl} = P_{Na}\Gamma_{Na} + P_{Cl}\Gamma_{Cl} \tag{3.17}$$

We assume the following equation to be true

$$P_{Na} = \frac{Z_{eff}^{Na}}{Z_{eff}^{Na} + Z_{eff}^{Cl}} \tag{3.18}$$

Using the table values for the effective Zs (table 1.1) we obtain $P_{Na} = 41\%$ and $P_{Cl} = 59\%$ that, together with the $\Gamma$s in equation 3.17, give:

$$\tau_{NaCl} = 0.717 \pm 0.002\,\mu s \tag{3.19}$$

As was the case for aluminum, we parametrize the histogram with:

$$N(t) = N_{free} e^{-\frac{t}{\tau_{free}}} + N_{NaCl} e^{-\frac{t}{\tau_{NaCl}}} + C \tag{3.20}$$

in which the first term takes into account muons decaying in detector 2, while the second term refers to those decaying in a bound state with NaCl. The last one is a background parameter. Given that the density of salt is lower than aluminum ($\rho_{Al} = 2.71\, g/cm^3$, $\rho_{NaCl} = 2.16\, g/cm^3$), we expect the ratio of decays in the bound state to be different than before.
We repeat the analysis as before. The result is shown in Figure 3.8.

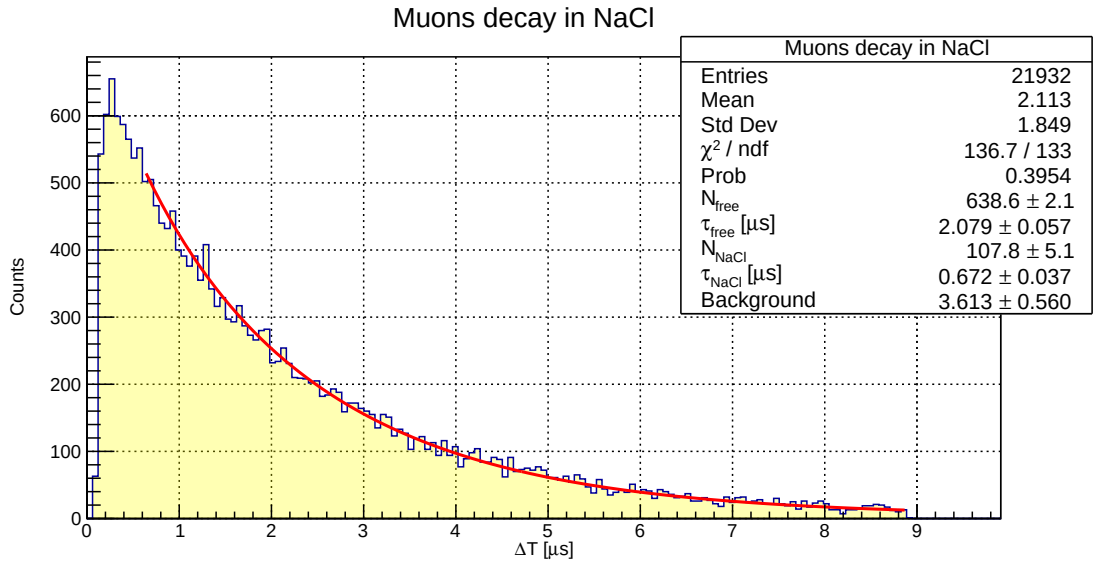


Figure 3.8: Muons decay in NaCl

We collected 21932 events in 140 hours. The result is:

$$\tau_{NaCl} = 0.672 \pm 0.037\,(stat)\,\mu s \tag{3.21}$$

We also evaluate muon lifetime considering separately up and down decays. The results are:

$$\begin{aligned} \tau^{up}_{NaCl} &= 0.672 \pm 0.039\,\mu s \\ \tau^{down}_{NaCl} &= 0.672 \pm 0.055\,\mu s \end{aligned} \tag{3.22}$$

The results, while in agreement with the previous one, are heavily affected by the fit process, this may be the reason why the two values are exactly the same.
Splitting the data in the Up and Down distribution reduces our statistics so the effect of the decay in the material is partially hidden by the free decay. For this reason we have to limit the parameters in order to simplify the fit process. The contribution of $\tau$ is greater than the other parameters so it is the most affected by the limits we have to impose.

# Chapter 4

# Asymmetry measurement in magnetic field

Cosmic muons are partially polarized because they are the result of pion decay. Pions being pseudoscalar mesons and assuming neutrinos to be eigenstates of elicity, we expect negative muons to be right-handed and positive muons to be left-handed. However, when measuring the angular distribution of the decay products to detect the asymmetry, only the positive muons will contribute.

## 4.1 Polarized $\mu^+$ decay

The $\mu^+$ decay amplitude is unaffected by the material:

$$\frac{d\Gamma_{\mu^+}}{d\cos\theta} = \frac{1}{2\tau^+}(1 + \frac{\xi}{3}\cos\theta) \tag{4.1}$$

in which $\xi$ (the mean polarization of cosmic muons, $\xi \approx 0.33$[5]) takes into account the kinetic depolarization (muons going opposite ways in the pion reference system will have the opposite polarization in the lab) and $\theta$ is the angle between the muon spin and the direction of the electron. By integrating in the upper and lower hemisphere of our detector ($\cos\theta \in$ [1,0], $\cos\theta \in$ [0,-1]) we obtain the following decay amplitudes:

$$\Gamma_{up} = \frac{1}{2\tau^+}(1 + \frac{\xi}{6}) \qquad \Gamma_{down} = \frac{1}{2\tau^+}(1 - \frac{\xi}{6}) \tag{4.2}$$

We define the asymmetry term:

$$A = \frac{N_u - N_d}{N_u + N_d} = \frac{\Gamma_{up} - \Gamma_{down}}{\Gamma_{up} + \Gamma_{down}} \tag{4.3}$$

So we expect a greater number of positive muons decays to be detected by the first detector rather than by the third.

## 4.2 $\mu^-$ depolarization

On the other hand, the negative muons lose almost all of their polarization due to processes happening during the shower and after being captured by the nuclei. In particular,

radiative transitions depolarize the $\mu^-$ down to 20% of the original polarization and even lower in the eventuality that the spin of the nucleus is nonzero. We will then assume the negative muons to be completely depolarized while measuring the asymmetry of the decay.

## 4.3 Magnetic field

To better measure the Asymmetry term we put the second detector in a magnetic field. That causes the muon spin to start preceding around the field lines with frequency:

$$\omega = g\frac{eB}{2m_\mu} \tag{4.4}$$

in which g is $\sim 2$ for a Dirac fermion. That changes the decay amplitude for the positive muons too:

$$\frac{d\Gamma_{\mu^+}}{d\cos\theta} = \frac{1}{2\tau^+}(1 + \frac{\xi}{3}\cos\theta\cos\omega t) \tag{4.5}$$

and the probability for the resulting electron to be revealed by the first (U) or the third (D) detector also depends on t:

$$U(t) = \frac{\Gamma_{up}}{\Gamma_{tot}} = \frac{1}{2}(1 + \frac{\xi}{6}\cos\omega t) \qquad D(t) = \frac{\Gamma_{down}}{\Gamma_{tot}} = \frac{1}{2}(1 - \frac{\xi}{6}\cos\omega t) \tag{4.6}$$

### 4.3.1 Experimental setup

To generate the magnetic field we use a $30 \times 80 \times 8.5$ cm solenoid consisting in a metallic case wrapped in copper wire. The detector must be rotated 90º to fit between the other two scintillators without them resting directly on top of each other. That greatly reduces the detection rate but is unavoidable to keep the solenoid from overheating or destroying the bottom detector with its heavy weight.

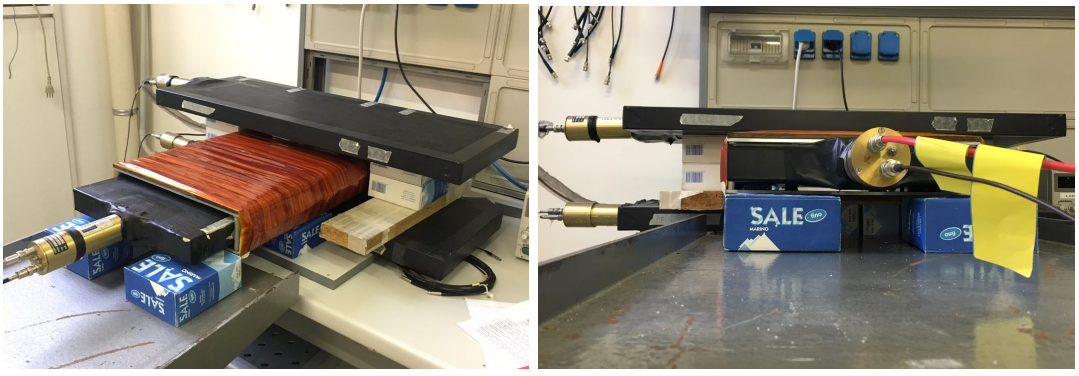


(a) Solenoid configuration: corner view. (b) Solenoid configuration: frontal view.

The copper wire is connected to a generator; the current intensity can be chosen through a set of knobs. In the approximation of an infinite solenoid, the magnetic field B is completely parallel to the surfaces and follows:

$$B = \frac{\mu_0 NI}{L} \tag{4.7}$$

in which $\mu_0$ is the magnetic permeability of the void, N is the number of loops, I is the current and L is the length of the solenoid.
The oscillation frequency $\omega$ depends on B, so we need a magnetic field strong enough to make the spin complete at least two entire oscillations (to have two maxima and two minima) during the time frame of the observation ($T \sim 9\,\mu s$). Having fewer oscillations could produce inconclusive results, while having more would mean sampling fewer bins at a time, greatly increasing the statistical fluctuations of the measurement. We need

$$\omega_{lim} = 2\left(\frac{2\pi}{T}\right) \approx 1.396\,Mrad/s \tag{4.8}$$

In the end, we choose B to be $\sim 20\,\mathrm{G}$, supplying 7.0 A from the generator. From 4.4, $\omega \approx 1.7\,\mathrm{Mrad/s}$ so we expect to see $\sim 2.46$ oscillations in $9\,\mu s$.

### 4.3.2 Characterization

Ideally we must ensure that the magnetic field is sufficiently uniform, especially in the central region which houses the sensitive part of the detector. We measure the intensity of the field with a Hall probe. We initially place the probe in the center of the solenoid and vary the electrical current supplied by the generator.

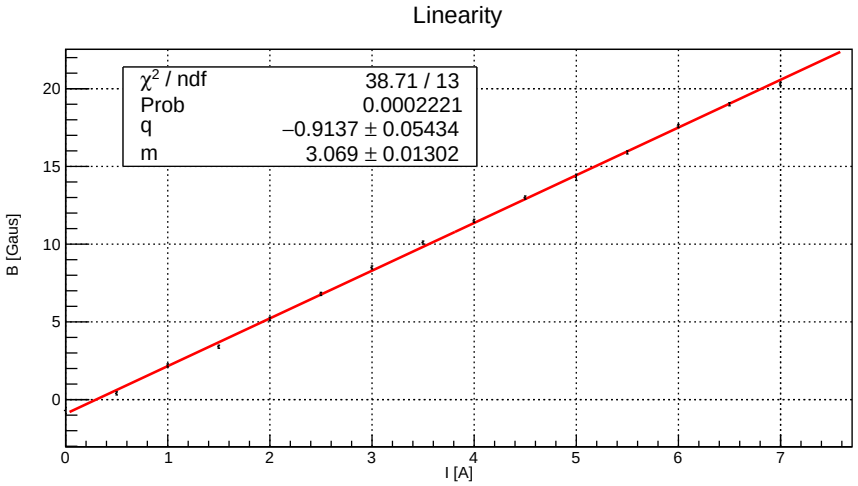


Figure 4.1: Magnetic field linearity. We used the sensibility of the probe as the error for the magnetic field.

Having chosen an intensity of $\sim$20 G for the field, we end up supplying I= 7 A to the solenoid. We then map the field in a $5 \times 5\,\mathrm{cm}$ grid, spanning the entirety of the solenoid and keeping the intensity of the current constant.

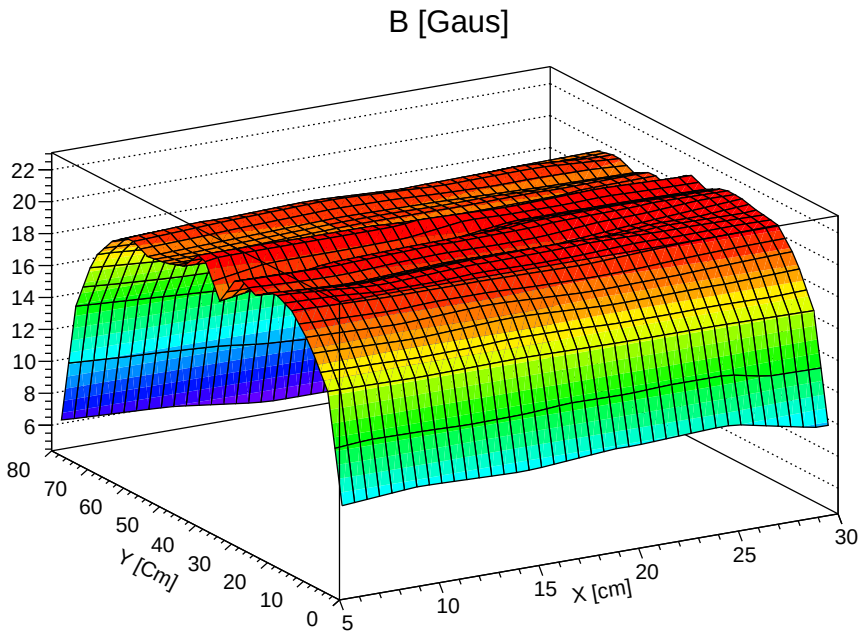


Figure 4.2: Magnetic field uniformity.

As shown in figure 4.2, the field is sufficiently uniform in the central region, especially along direction X, while when getting close to the borders along Y, the intensity decreases rapidly. The average intensity of the field in the central region is $20.2 \pm 0.8\,\mathrm{G}$ which corresponds to:

$$\omega = (1.72 \pm 0.07) \times 10^6\, rad/s \tag{4.9}$$

## 4.4 Asymmetry measurement

With our experimental setup we see the effects of both the positive polarized muons and the negative unpolarized muons, that must be taken into account when calculating the expected asymmetry:

$$A(t) = \frac{U(t) - D(t)}{U(t) + D(t)} \tag{4.10}$$

in which U(t) and D(t) stand, respectively, for the probability of having a stop signal in the $1^{st}$ detector or in the $3^{rd}$ one.

$$U(t) = \frac{0.56\Gamma(t)^u_{\mu^+} + 0.44\Gamma(t)^u_{\mu^-}}{\Gamma_{tot}} \qquad D(t) = \frac{0.56\Gamma(t)^d_{\mu^+} + 0.44\Gamma(t)^d_{\mu^-}}{\Gamma_{tot}} \tag{4.11}$$

$$\begin{aligned} U(t) &= \frac{1}{\Gamma_{tot}}(0.56[\frac{1}{2\tau^+}(1 + \frac{\xi}{6}\cos\omega t] + 0.44\frac{1}{\tau^-}) \\ D(t) &= \frac{1}{\Gamma_{tot}}(0.56[\frac{1}{2\tau^+}(1 - \frac{\xi}{6}\cos\omega t] + 0.44\frac{1}{\tau^-}) \end{aligned} \tag{4.12}$$

$$A(t) = \frac{\xi}{6}\cos\omega t[\frac{\tau^-}{\tau^- + \frac{0.44}{0.56}\tau^+}] = 0.54\,\frac{\xi}{6}\cos\omega t \simeq 0.03\cos\omega t \tag{4.13}$$

We will compare this value with the measured:

$$A(t) = \frac{N_u - N_d}{N_u + N_d} \tag{4.14}$$

We managed to collect about 60,000 events, so we should choose a binning so that the statistical fluctuations of bins that count towards the first maximum and minimum are significantly shorter than the amplitude of the oscillation. The standard deviation on A, assuming, for each bin, $\sigma_{N_{u/d}} = \sqrt{N_{u/d}}$, is:

$$\sigma_A = \sqrt{\frac{4N_u^2 N_d}{(N_u + N_d)^4} + \frac{4N_d^2 N_u}{(N_u + N_d)^4}} = \sqrt{\frac{4N_u N_d}{(N_u + N_d)^3}} \tag{4.15}$$

We want that:

$$\sigma_A < \frac{\xi}{6} \times 0.54 \simeq 0.03 \tag{4.16}$$

$N_{tot} = N_u + N_d$ being the total number of counts in the bin, we need it to be greater than $\sim 1000$.

### 4.4.1 Experimental Results

We collected 60,000 events in over a month of data taking. The examined batch is the result of 4 smaller sampling intervals, due to unfortunate power shortages. We have no reason to believe that the latter affected our setup, since there were no visible changes in the detection rate.

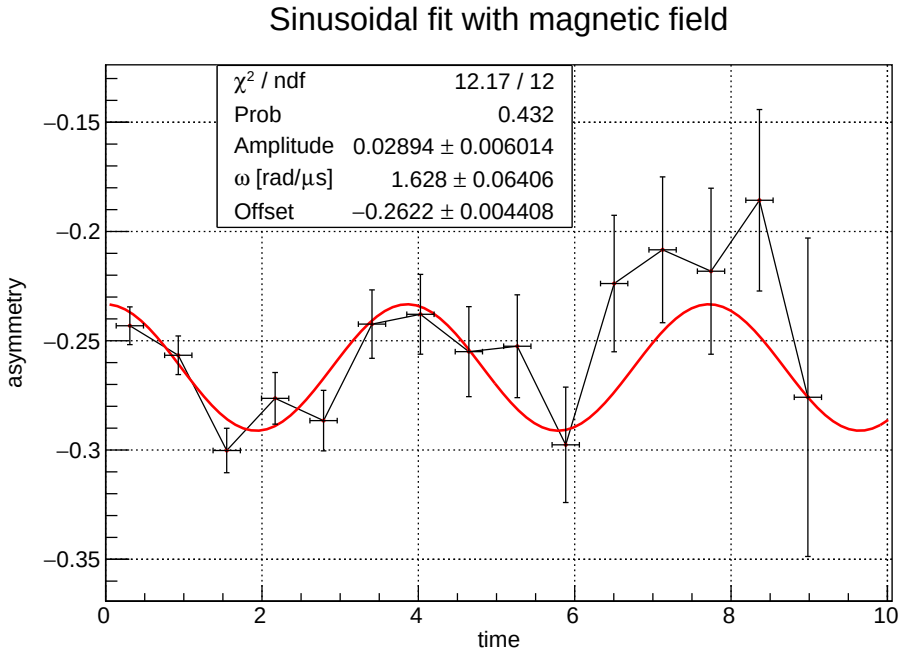


Figure 4.3: Asymmetry of the decay in the presence of a magnetic field.

The binning was chosen by running the analysis from 6 up to 30 bins. In figure 4.3 the best result is shown.

We obtained:

$$\xi = 0.32 \pm 0.07 \tag{4.17}$$

$$\omega = (1.63 \pm 0.06)\ Mrad/s \tag{4.18}$$

Both are well within expectations. On the same graph we also tested the hypothesis of no magnetic field, that resulted unconvincing.

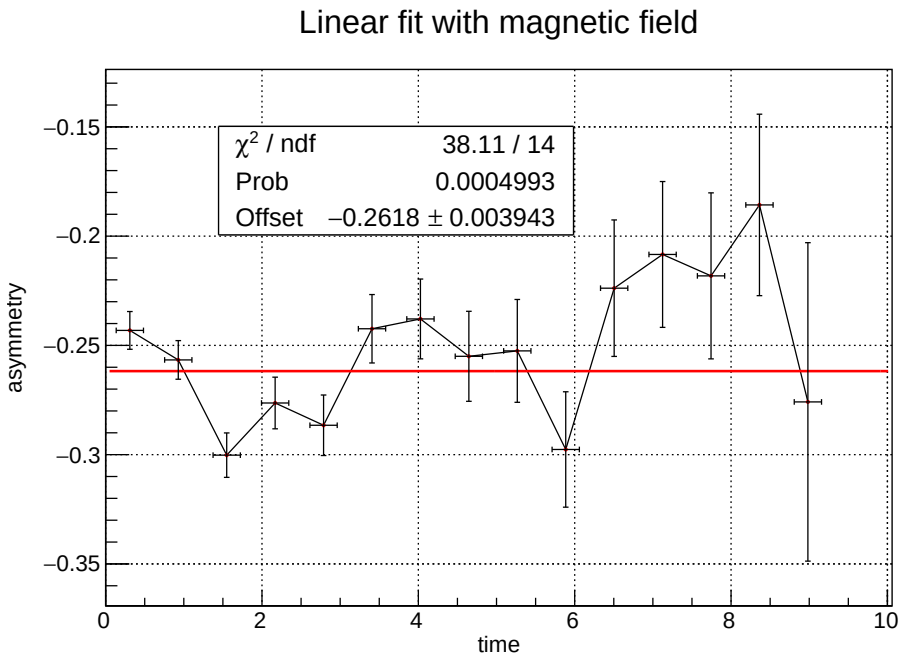


Figure 4.4: Hypothesis of no magnetic field in the presence of one.

To be certain the results aren't due to statistical fluctuations, we also analyzed the data batch of section 3.1.1, acquired in the absence of a magnetic field.

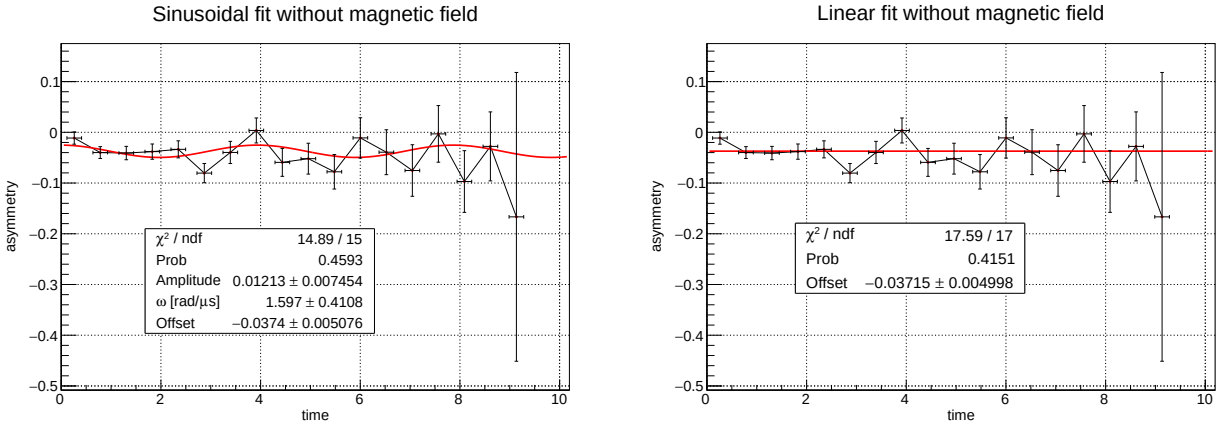


(a) Hypotesis of magnetic field in the absence of one. (b) Hypotesis of no magnetic field in the absence of one.

In this case the results indicate, as expected, that there's no magnetic field. The solenoid seems to introduce a preference between the two detectors as most electrons are consistently detected by scintillator 3, as indicated by the offset parameter. This is probably caused by the geometry of the setup, rather than by the actual magnetic field.

# Conclusions

Although we cannot completely justify an offset significantly different from 0, the measurement of muon polarization, and consequently of parity violation, can be considered trustworthy, given the compatibility with the expected values.

# Bibliography


[1] Alessandro Bettini. *Introduction to elementary particle physics*. Cambridge University Press, 2014.

[2] T. Suzuki, D. F. Measday, and J. P. Roalsvig. Total nuclear capture rates for negative muons. *Phys. Rev. C*, 35:2212–2224, Jun 1987.

[3] Glenn E Knoll. *Radiation Detection and Measurement Third Edition*. University of Michigan, 1999.

[4] N. Y. Agafonova, M. Aglietta, P. Antonioli, G. Bari, R. Bertoni, V. V. Boyarkin, E. Bressan, G. Bruno, V. L. Dadykin, E. A. Dobrynina, R. I. Enikeev, W. Fulgione, P. Galeotti, M. Garbini, P. L. Ghia, P. Giusti, E. Kemp, A. S. Malgin, B. Miguez, A. Molinario, R. Persiani, I. A. Pless, V. G. Ryasny, O. G. Ryazhskaya, O. Saavedra, G. Sartorelli, M. Selvi, G. C. Trinchero, C. Vigorito, V. F. Yakushev, and A. Zichichi. *"Measurement of cosmic muon charge ratio with the Large Volume Detector"*. *ArXiv e-prints*, November 2013.

[5] C. Scott Johnson. Polarization of cosmic-ray muons at sea level. *Phys. Rev.*, 122:1883–1890, Jun 1961.

[6] D.F. Measday. The nuclear physics of muon capture. 354:243–409, 11 2001.